Physics – Uspekhi **56** (4) 321 – 346 (2013)

REVIEWS OF TOPICAL PROBLEMS PACS numbers: 95.30.Lz, 97.10.Gz, 97.80.Jp, 98.70.Qy

Quasispherical subsonic accretion in X-ray pulsars

N I Shakura, K A Postnov, A Yu Kochetkova, L Hjalmarsdotter

DOI: 10.3367/UFNe.0183.201304a.0337

Contents

Abstract. **A theoretical model is considered for quasispherical subsonic accretion onto slowly rotating magnetized neutron stars. In this regime, the accreting matter settles down subsonically onto the rotating magnetosphere, forming an extended quasistatic shell. Angular momentum transfer in the shell occurs via large-scale convective motions resulting, for observed pulsars, in an almost iso-angular-momentum $\omega \sim 1/R^2$ rotation law inside the shell. The accretion rate through the shell is determined by the ability of the plasma to enter the magnetosphere due to Rayleigh–Taylor instabilities, with allowance for cooling. A settling accretion regime is possible for moderate accretion rates $\dot{M} \lesssim \dot{M}_* \simeq 4 \times 10^{16}$ g s^{-1}. At higher accretion rates, a free-fall gap above the neutron star magnetosphere appears due to rapid Compton cooling, and the accretion becomes highly nonstationary. Observations of spin-up/spin-down rates of quasispherically wind accreting equilibrium X-ray pulsars with known orbital periods (e.g., GX 301-2 and Vela X-1) enable us to determine the main dimensionless parameters of the model, as well as to estimate surface magnetic field of the neutron star. For equilibrium pulsars, the independent measurements of the neutron star magnetic field allow for an estimate of the stellar wind velocity of the optical companion without using complicated spectroscopic measurements. For nonequilibrium pulsars, a maximum value is shown to exist for the spin-down rate of the accreting neutron star. From observations of the spin-down rate and the X-ray luminosity in such pulsars (e.g., GX 1 + 4, SXP 1062, and 4U 2206 + 54), a lower limit can be put on the neutron star magnetic field, which in all cases turns out to be close to the standard value and which agrees with cyclotron line measurements. Furthermore, both explains the spin-up/spin-down of the pulsar frequency on large time-scales and also accounts for the irregular short-term frequency fluctuations, which may correlate or anticorrelate with the observed X-ray luminosity fluctuations.**

N I Shakura, K A Postnov, A Yu Kochetkova, L Hjalmarsdotter
Sternberg State Astronomical Institute,
Lomonosov Moscow State University,
Universitetskii prosp. 13, 119992 Moscow, Russian Federation
E-mail: kpostnov@gmail.com

Received 16 August 2012, revised 23 November 2012
Uspekhi Fizicheskikh Nauk **183** (4) 337 – 364 (2013)
DOI: 10.3367/UFNr.0183.201304a.0337
Translated by K A Postnov; edited by A Radzig

1. Introduction

X-ray pulsars are highly magnetized rotating neutron stars (NSs) in close binary systems, accreting matter from a companion star. The companion may be a low-mass star overfilling its Roche lobe, in which case an accretion disc forms. In the case of a high-mass early type companion, the neutron star may also accrete from a strong stellar wind, and depending on the conditions a disc may be formed or accretion may proceed quasispherically. The strong magnetic field (on the order of $10^{12}-10^{13}$ G) of the neutron star disrupts the accretion flow at some distance from the neutron star surface and forces the accreted matter to funnel down on the polar caps of the neutron star, creating hot spots. If the magnetic dipole axis is misaligned with the rotational axis, then the neutron star pulsates in X-rays. Most accreting pulsars show stochastic variations in their spin frequencies, as well as in their luminosities. Many sources also exhibit long-term trends in their spin-behavior, with the period more or less steadily increasing or decreasing, and in some sources spin-reversals have been observed. (For a thorough review, see, e.g., Ref. [1] and references cited therein.)

The best-studied case of accretion is that of thin disc accretion [2]. Here, the spin-up/spin-down mechanisms are rather well understood. For disc accretion, the spin-up torque is determined by the specific angular momentum at the inner edge of the disc and can be written in the form [3] $K_{\rm su} \approx \dot{M}\sqrt{GMR_{\rm A}}$, where G is the gravitational constant, M is the mass of the neutron star, and $\dot{M} \equiv {\rm d}M/{\rm d}t$ is the accretion rate. For a pulsar, the inner radius of the accretion disc is determined by the Alfvén radius $R_{\rm A} \sim \dot{M}^{-2/7}$, so $K_{\rm su} \sim \dot{M}^{6/7}$, i.e., for disc accretion the spin-up torque is weakly (almost linearly) dependent on the accretion rate (X-ray luminosity). In contrast, the spin-down torque for disc accretion is independent of $\dot{M}$ in the first approximation: $K_{\rm sd} \sim -\mu^2/R_{\rm c}^3$, where $R_{\rm c} = (GM/\omega^{*2})^{1/3}$ is the corotation radius, ω^* is the neutron star angular frequency, and μ is the neutron star's dipole magnetic moment. Actually, accretion torques in disc accretion are determined by complex disc–magnetosphere interactions (see, e.g., Refs [4, 5] and the discussion in paper [6]), and correspondingly can have a more complicated dependence on the mass accretion rate and other parameters.

Measurements of spin-up/spin-down in X-ray pulsars can be used to evaluate a very important parameter of the neutron star, namely its magnetic field. The period of the pulsar spin is usually close to the equilibrium value $P_{\rm eq}$ whereat the total torque applied to the neutron star is equal to zero: $K = K_{\rm su} + K_{\rm sd} = 0$. So, assuming the observed value of the neutron star spin frequency equal to $\omega^* = 2\pi/P_{\rm eq}$, the magnetic field of the neutron star in disc-accreting X-ray pulsars can be estimated if $\dot{M}$ is known.

In the case of quasispherical accretion, which may take place in binary systems where the optical star underfills its Roche lobe and no accretion disc is formed, the situation is more complicated. Clearly, the magnitude and sign of the angular momentum supplied to the neutron star from the captured stellar wind are important for its spin-up or spin-down. To within a numerical factor on the order of 1 (which can be either positive or negative; see numerical simulations in papers [7–9], etc.), the torque applied to the neutron star in this case should be proportional to $\dot{M}\omega_{\rm B}R_{\rm B}^2$, where $\omega_{\rm B} = 2\pi/P_{\rm b}$ is the binary orbital angular frequency, $P_{\rm b}$ is the orbital period of a binary, $R_{\rm B} = 2GM/(V_{\rm w}^2 + v_{\rm orb}^2)$ is the gravitational capture (Bondi) radius, $V_{\rm w}$ is the stellar wind velocity at the neutron star orbital distance, and $v_{\rm orb}$ is the neutron star orbital velocity. In real high-mass X-ray binaries, the orbital eccentricity is nonzero, the stellar wind is variable and can be inhomogeneous, etc., so $K_{\rm su}$ can be a composite function of time. The spin-down torque then appears to be even more uncertain, since it is impossible to write down for it a simple expression like $-\mu^2/R_{\rm c}^3$ any more ($R_{\rm c}$ has no clear meaning for quasispherical accretion; it is much larger in slowly rotating pulsars than the Alfvén radius whereat the angular momentum transfer from the accreting matter to the magnetosphere actually occurs). For example, using the expression $-\mu^2/R_{\rm c}^3$ for the braking torque results in a very high ($\gtrsim 10^{14}$ G) magnetic field for long-period X-ray pulsars. We think this is a result of underestimating the braking torque.

Matter captured from the stellar wind can accrete onto the neutron star in different ways. Indeed, if the X-ray flux from the accreting neutron star is sufficiently high, the shocked matter rapidly cools down due to Compton processes and falls freely toward the magnetosphere. The velocity of motion of the impinging matter rapidly becomes supersonic, so a shock is formed above the magnetosphere. This accretion regime was considered, for example, in Ref. [10]. Depending on the sign of the specific angular momentum of falling matter (prograde or retrograde), the neutron star can spin up or spin down. However, if the X-ray flux at the Bondi radius is below a certain value, the shocked matter remains hot, the radial velocity of the plasma is subsonic, and the source may enter the settling accretion regime. A hot quasispherical shell forms around the magnetosphere [11] (Fig. 1). Due to additional energy release (especially near the base of the shell), the temperature gradient across the shell becomes superadiabatic, and large-scale convective motions inevitably occur. The convection generates turbulence, and the motion of a fluid element in the shell becomes quite complicated. If the magnetosphere allows plasma entry via instabilities (and

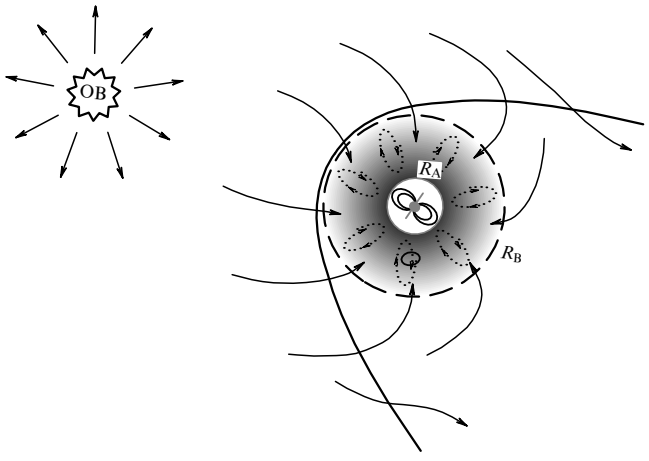

Figure 1. A schematic of quasispherical accretion from the stellar wind of an optical companion OB star (left) onto a magnetized neutron star (right) in a binary system. In the regime of subsonic accretion, a quasispherical shell (shaded area) of radius $R_{\rm A}$ is formed between the bow shock (parabolic curve) and the rotating magnetosphere. In this shell, large-scale convective motions develop that may act to withdraw angular momentum from the magnetosphere. The outer radius of the shell is determined by the gravitational capture or Bondi radius $R_{\rm B}$. The characteristic velocity of the wind is $v_{\rm w} \sim 300-1000$ km s^{-1}. The contour arrow shows the direction of the orbital velocity $v_{\rm orb}$ of the neutron star.

subsequent accretion onto the neutron star), the actual accretion rate through such a shell is controlled exactly by the magnetosphere (for example, a shell can exist in certain conditions, but accretion through it can be weak or even absent altogether).

On top of the convective motions, therefore, the matter acquires a low, on average radial, velocity toward the magnetosphere, and thus subsonic settling is established. This type of accretion can work only for relatively small X-ray luminosities, $L_X < 4 \times 10^{36}$ erg s^{-1} (see Section 2.3 and Appendix E), and is totally different from that considered in the numerical simulations cited above. If a shell is present, its interaction with the rotating magnetosphere can lead to spin-up or spin-down of the neutron star, depending on the sign of the difference between the angular velocities of the accreting matter and the magnetospheric boundary. Thus, both spin-up and spin-down of the neutron star is possible in the settling accretion regime, even if the sign of the specific angular momentum of the captured matter is always prograde. The shell here mediates the angular momentum transfer to or from the rotating neutron star.

There are several models in the literature (see especially papers [12, 13]), from which the expression for the spin-down torque for quasispherically accreting neutron stars in the form $K_{sd} \sim -\dot{M}R_A^2\omega^*$ can be derived. Substituting the standard expression for the Alfén radius, $R_A \sim \dot{M}^{-2/7}\mu^{4/7}$, this torque is transformed to $K_{sd} \sim -\mu^{8/7}\dot{M}^{3/7}$. In our model, the matter in the shell settles subsonically as the region close to the magnetospheric surface cools down, and the Alfvén radius has a different dependence on the mass accretion rate and the magnetic field: $R_A \sim \dot{M}^{-2/11}\mu^{6/11}$ (see Sections 2.2 and 2.3).

It can be shown that there are two different mechanisms through which angular momentum can be transferred through a quasispherical shell. In the first case (we call this case *moderate coupling*), angular momentum is withdrawn by convective motions in the shell. The braking torque in the regime of settling accretion with convective removal of angular momentum depends on the accretion rate as $K_{sd} \sim -\dot{M}^{3/11}$ (see Section 4). The characteristic velocity of the convective motions in this regime is close to the speed of sound. It is also possible to describe a settling regime where the angular momentum is removed by shear turbulence in the shell (the *weak coupling* regime). In this regime, the characteristic velocities of the shear flow close to the magnetosphere are on the order of magnitude of the linear rotational velocity. In this case, $K_{sd} \sim \mu^2/R_c^3 \sim \mu^2\omega^{*2}/(GM)$, i.e., in the weak coupling regime the torque does not depend on the accretion rate at all.

To stress the difference between the two possible regimes of subsonic accretion (with moderate and weak coupling), let us rewrite the expression for the braking torque with due regard for convection (moderate coupling) in terms of the corotation radius and the Alfvén radius:

$$K_{sd} \sim -\frac{\mu^2}{\sqrt{R_c^3 R_A^3}} \sim -\frac{\mu^2}{R_c^3}\left(\frac{R_c}{R_A}\right)^{3/2}$$

(see further details in Section 3). Because the factor $(R_c/R_A)^{3/2} \sim (\omega_K(R_A)/\omega^*)$, where ω_K is the Keplerian angular velocity, can be of order 10 or more in real systems, using a braking torque in the form of μ^2/R_c^3 may lead to a strong overestimation of the magnetic field strength for the neutron star.

The dependence of the braking torque on the accretion rate in the case of quasispherical settling accretion suggests that variations of the mass accretion rate (and X-ray luminosity) must lead to a change in the accretion regime from acceleration (at high accretion rates) to deceleration (at low accretion rates) at some critical value of $\dot{M}$ (or R_A), which differs from source to source. This phenomenon (known as torque reversal) is actually observed in wind-fed pulsars like Vela X-1, GX 301-2, and GX 1+4, which we shall consider below in more detail.

The layout of this review is as follows. In Section 2, we present an outline of the theory of quasispherical accretion onto a neutron star magnetosphere. We show that it is possible to construct a hot envelope around the neutron star through which subsonic accretion will occur and act to either spin up or spin down the neutron star. At the end of this section, we also discuss the structure of the interchange instability region, which determines the rate of plasma entering into the magnetosphere of the rotating neutron star. In Section 3, the angular momentum transfer to the magnetosphere is treated. In the next Section 4, we consider how the spin-up/spin-down torques vary with changing accretion rate and how to determine the parameters of quasispherical accretion from observational data. In Section 5, we apply our methods to analyzing the specific pulsars GX 301-2, Vela X-1, GX 1+4, SXP 1062, and 4U 2206+54. In Section 6, we examine our results and, finally, present our conclusions in Section 7. A detailed gas-dynamic treatment of the problem is presented in Appendices A–E, which is very important for understanding the physical processes proceeding in the shells. This work follows to a large extent the earlier published paper [14]. However, many additions clarifying and refining the physical model (especially in Sections 2–4 and in the Appendices) are included here, and a comparison of the model with recent observations of several X-ray pulsars is also made.

2. Quasispherical accretion

2.1 Structure of a subsonic shell around a neutron star magnetosphere

We shall here look at the torques applied to a neutron star in the case of quasispherical accretion from a stellar wind. Wind matter is gravitationally captured by the moving neutron star, and a bow shock is formed at a characteristic distance $R \sim R_B$, where R_B is the Bondi radius. Angular momentum can be removed from the neutron star magnetosphere in two ways: either with matter expelled from the magnetospheric boundary without accretion (the propeller regime [15]) or via large-scale convective motions in a subsonic quasistatic shell around the magnetosphere, in which case the accretion rate onto the neutron star is determined by the ability of the plasma to extend through the magnetosphere in the regime of subsonic accretion.

In such a quasistatic shell, the temperature will be high (on the order of the virial temperature; see paper [11]), and the important point is whether hot matter from the shell can in fact enter the magnetosphere. Two-dimensional calculations in Ref. [16] have shown that hot monatomic ideal plasma is stable relative to the Rayleigh–Taylor instability at the magnetospheric boundary, and plasma cooling is thus needed for accretion to begin. However, a closer inspection of the three-dimensional calculations in Ref. [17] revealed that

the hot plasma is only marginally stable at the magnetospheric equator (within 5% accuracy of their calculations). Compton cooling and the possible dissipative phenomena (magnetic reconnection, etc.) facilitate the plasma penetration into the magnetosphere. We will show in Section 3 that spin-down of the neutron star is possible in the case of accretion of matter from a hot envelope in the subsonic settling regime.

In a zeroth approximation, we can neglect both rotation and radial motions (accretion) of matter in the shell and consider only its equilibrium hydrostatic structure. The radial velocity u_r of matter falling through the shell is lower than the sound velocity c_s. Under these assumptions, the characteristic cooling/heating timescale is much larger than the free-fall timescale.

In general, both gas pressure and anisotropic turbulent motions are present in the shell, and therefore Pascal's law is violated. Then, the hydrostatic equilibrium equation can be derived from the equation of motion (A.16) with stress tensor components (A.19)–(A.21) and zero viscosity (see Appendix A for more details):

$$-\frac{1}{\rho}\frac{\mathrm{d}P_g}{\mathrm{d}R}-\frac{1}{\rho R^2}\frac{\mathrm{d}(P_\parallel^t R^2)}{\mathrm{d}R}+\frac{2P_\perp^t}{\rho R}-\frac{GM}{R^2}=0\,. \tag{1}$$

Here, $P_g=\rho c_s^2/\gamma$ is the gas pressure, and P^t stands for the pressure due to turbulent motions:

$$P_\parallel^t=\rho\langle u_\parallel^2\rangle=\rho m_\parallel^2 c_s^2=\gamma P_g m_\parallel^2\,, \tag{2}$$

$$P_\perp^t=\rho\langle u_\perp^2\rangle=\rho m_\perp^2 c_s^2=\gamma P_g m_\perp^2\,, \tag{3}$$

where $\langle u_t^2\rangle=\langle u_\parallel^2\rangle+2\langle u_\perp^2\rangle$ is the turbulent velocity dispersion, and $m_\parallel^2$ and $m_\perp^2$ are turbulent Mach numbers squared in the radial and tangential directions, respectively; for example, in the case of isotropic turbulence one has $m_\parallel^2=m_\perp^2=(1/3)m_t^2$, where m_t is the turbulent Mach number. The total pressure is the sum of the gas and turbulence terms: $P_g+P^t=P_g(1+\gamma m_t^2)$. The turbulent Mach number in the shell may, in general, depend on the radius. In our case, however, we will consider it constant. Furthermore, the inclusion of turbulent heating (important from a dynamic point of view; see Appendix E) in real pulsars will change the estimated parameters by less than a factor of 2 (see appropriate formulas in Section 4).

We shall consider, to a first approximation, that the entropy S is constant throughout the shell. For an ideal gas with adiabatic index γ and equation of state $P=K\exp(S/c_V)\rho^\gamma$, the density can be expressed as a function of temperature: $\rho\sim T^{1/(\gamma-1)}$. Integrating the hydrostatic equilibrium equation (1) then yields

$$\frac{\mathcal{R}T}{\mu_m}=\frac{\gamma-1}{\gamma}\frac{GM}{R}\frac{1}{1+\gamma m_\parallel^2-2(\gamma-1)(m_\parallel^2-m_\perp^2)}$$

$$=\frac{\gamma-1}{\gamma}\frac{GM}{R}\psi(\gamma,m_t)\,, \tag{4}$$

where $\mathcal{R}$ is the universal gas constant, and μ_m is the molecular weight. (In this solution we have neglected the integration constant, which is not important deep inside the shell. It is important in the outer part of the shell, but since the outer region close to the bow shock at $\sim R_B$ is not spherically symmetric, its structure can only be found numerically.)

It should be noted that taking turbulence into account somewhat decreases the temperature within the shell. Most important, however, is that the anisotropy of turbulent motions, caused by convection, in the stationary case changes the distribution of angular velocity of matter rotation in the shell. We will show below in Appendices B and C that, in the case of isotropic turbulence, the angular velocity distribution within the shell is close to quasi-Keplerian: $\omega(R)\sim R^{-3/2}$. In the case of strongly anisotropic turbulence caused by convection, $m_\parallel^2\gg m_\perp^2$, the distribution of momentum in the shell may become almost iso-angular: $\omega(R)\sim R^{-2}$. In Section 5, we shall see that an analysis of several real X-ray pulsars favors an iso-angular-momentum rotation distribution.

Now, let us write down how the density varies inside the quasistatic shell for $R\ll R_B$. For a fully ionized gas with $\gamma=5/3$, we find the law of density change:

$$\rho(R)=\rho(R_A)\left(\frac{R_A}{R}\right)^{3/2}, \tag{5}$$

and the law of gas pressure variation:

$$P(R)=P(R_A)\left(\frac{R_A}{R}\right)^{5/2}. \tag{6}$$

The above equations describe the structure of an ideal static adiabatic shell above the magnetosphere. Of course, the problem becomes essentially nonspherically symmetric at $R\sim R_B$, and numerical simulations are required for calculating the structure of shell's outer parts.

Corrections to the adiabatic temperature gradient due to convective energy transport through the shell are evaluated in Appendix D.

2.2 Alfvén surface

At the magnetospheric boundary (the Alfvén surface), the total pressure (including isotropic gas pressure and the possibly anisotropic turbulent pressure) is balanced by the magnetic field pressure $B^2/(8\pi)$:

$$P_g+P_t=P_g(R_A)(1+\gamma m_t^2)=\frac{B^2(R_A)}{8\pi}\,. \tag{7}$$

The magnetic field at the Alfvén radius is determined by the dipole magnetic moment of the neutron star and by electric currents flowing along the Alfvénic surface (in the magnetopause):

$$P_g(R_A)=\frac{K_2}{(1+\gamma m_t^2)}\frac{B_0^2}{8\pi}\left(\frac{R_0}{R_A}\right)^6=\frac{\rho\mathcal{R}T}{\mu_m}\,, \tag{8}$$

where the dimensionless coefficient K_2 takes into account the contribution from these currents, and the factor $1/(1+\gamma m_t^2)$ is due to the turbulent pressure term. For example, in the model constructed by Arons and Lea [17] [see their Eqn (31)], $K_2=(2.75)^2\approx 7.56$. At the magnetospheric cusp (where the magnetic force line is branched), the radius of the Alfvén surface is about 0.51 times that of the equatorial radius [17]. Below, we shall assume that R_A stands for the equatorial radius of the magnetosphere, unless stated otherwise.

Plasma is able to penetrate into the magnetosphere mainly due to the interchange instability. In the stationary regime, let us introduce the accretion rate $\dot{M}$ onto the neutron star

surface. From the continuity equation in the shell we find

$$\rho(R_A) = \frac{\dot{M}}{4\pi u_r(R_A) R_A^2} . \quad (9)$$

Clearly, the velocity of matter absorption by the magnetosphere is smaller than the free-fall velocity, so we introduce a dimensionless factor $f(u) = u_r/\sqrt{2GM/R} < 1$. Then, the density at the magnetospheric boundary is given by

$$\rho(R_A) = \frac{\dot{M}}{4\pi f(u)\sqrt{2GM/R_A}\, R_A^2} . \quad (10)$$

For example, $f(u) \approx 0.1$ in the model calculations [17]; in our case, the value of $f(u)$ at high X-ray luminosities may attain ≈ 0.5. If we imagine that the shell is impenetrable and that there is no accretion through it, $\dot{M} \to 0$, then $u_r \to 0$, $f(u) \to 0$, while the density in the shell remains finite. In some sense, matter leaks from the magnetosphere down onto the neutron star, and the leakage may be either very small ($\dot{M} \to 0$) or have a finite nonzero value ($\dot{M} \neq 0$).

Plugging $\rho(R)$ into formula (8) and using relationship (4) and the definition of the dipole magnetic moment,

$$\mu = \frac{1}{2} B_0 R_0^3 ,$$

(where R_0 is the neutron star radius), we find an expression for the Alfvén radius in the case of quasispherical accretion:

$$R_A = \left[\frac{4\gamma}{(\gamma-1)} \frac{f(u) K_2}{\psi(\gamma, m_t)(1+\gamma m_t^2)} \frac{\mu^2}{\dot{M}\sqrt{2GM}} \right]^{2/7} . \quad (11)$$

It should be stressed that in the presence of a hot shell the Alfvén radius is determined by the static gas pressure (with a possible addition of turbulent motions) at the magnetospheric boundary, which is nonzero even for a zero-mass accretion rate through the shell. The dependence of $f(u)$ on the accretion rate $\dot{M}$ in the case of a settling shell taking cooling into account will be derived below [see formula (32) below]. In the supersonic (Bondi) regime, we obviously have $f(u) = 1$. Notice that accretion with subsonic velocity can take place even in the Bondi regime [18], but with a significantly lower accretion rate (as compared to the maximum). In the Bondi regime (i.e., in the adiabatic regime without gas heating and/or cooling), the choice of solution depends on the boundary conditions.

2.3 Mean velocity of matter entering through the magnetospheric boundary

As mentioned in Section 2.2, plasma penetrates into the magnetosphere of a slowly rotating neutron star mainly due to the interchange instability. The boundary between the plasma and the magnetosphere will be stable at high temperatures $T > T_{cr}$, but becomes unstable for $T < T_{cr}$, and remains in a neutral equilibrium at $T = T_{cr}$ [16]. The critical temperature equals

$$\mathcal{R} T_{cr} = \frac{1}{2(1+\gamma m_t^2)} \frac{\cos\chi}{\kappa R_A} \frac{\mu_m G M}{R_A} . \quad (12)$$

Here, κ is the local curvature of the magnetosphere, χ is the angle the outer normal makes with the radius vector at a given point, and the contribution from turbulent pulsations in the plasma to the total pressure is taken into account by the factor $(1+\gamma m_t^2)$. The effective gravitational acceleration can be written down as

$$g_{eff} = \frac{GM}{R_A^2} \cos\chi \left(1 - \frac{T}{T_{cr}}\right) . \quad (13)$$

The temperature in the quasistatic shell is given by expression (4), and the condition for the magnetosphere instability can thus be rewritten as

$$\frac{T}{T_{cr}} = \frac{2(\gamma-1)(1+\gamma m_t^2)}{\gamma} \psi(\gamma, m_t) \frac{\kappa R_A}{\cos\chi} < 1 . \quad (14)$$

According to work [17], when the external gas pressure decreases with radius as $P \sim R^{-5/2}$, the form of the magnetosphere far from the polar cusp can be described to within 10% accuracy as $(\cos\lambda)^{0.2693}$ (here, λ is the polar angle counted from the magnetospheric equator). The instability first appears near the equator, where the curvature of magnetic lines is minimal. Near the equatorial plane ($\lambda = 0$), for a poloidal dependence of the magnetosphere defined approximately by $(\cos\lambda)^{0.27}$, we get for the curvature $\kappa_p R_A = 1 + 0.27$. The toroidal field curvature at the magnetospheric equator is $\kappa_t R_A = 1$. The tangent sphere at the equator cannot have a radius larger than the inverse poloidal curvature; whence it follows that $\kappa R_A = 1.27$ at $\lambda = 0$. This is somewhat larger than the value of $\kappa R_A = \gamma/(2(\gamma-1)) = 5/4 = 1.25$ (for $\gamma = 5/3$ in the absence of turbulence or for fully isotropic turbulence), but falls within the calculation accuracy limit.[1] The contribution from anisotropic turbulence decreases the critical temperature; for example, we obtain $T/T_{cr} \sim 2$ for $\gamma = 5/3$ in the case of strongly anisotropic turbulence $m_\parallel = 1$, $m_\perp = 0$ at $\lambda = 0$, i.e., anisotropic turbulence enhances the stability of the magnetosphere. Thus, the plasma-magnetospheric boundary is initially stable, and after cooling to $T < T_{cr}$ plasma instability sets in, starting in the equatorial zone where the curvature of the magnetospheric surface is minimal.

Let us consider the development of the interchange instability in plasmas when cooling (predominantly Compton cooling) is present. The temperature therewith changes as [20, 21]

$$\frac{dT}{dt} = -\frac{T - T_X}{t_C} , \quad (15)$$

where the Compton cooling time equals

$$t_C = \frac{3}{2\mu_m} \frac{\pi R_A^2 m_e c^2}{\sigma_T L_X} \approx 10.6\, R_9^2 \dot{M}_{16}^{-1}\ [\mathrm{s}] . \quad (16)$$

Here, m_e is the electron mass, σ_T is the Thomson cross section, $L_X = 0.1\dot{M}c^2$ is the X-ray luminosity, T is the electron temperature (which is equal to the ion temperature since the timescale of electron–ion energy exchange here is the shortest possible), T_X is the X-ray temperature, and $\mu_m = 0.6$ is the molecular weight of a fully ionized plasma with the solar chemical composition, and the following notation was introduced: $R_9 \equiv R/(10^9\ \mathrm{cm})$, $\dot{M}_{16} \equiv \dot{M}/(10^{16}\ \mathrm{g\ s^{-1}})$. The photon temperature is $T_X = (1/4)T_{cut}$ for a bremsstrahlung spectrum with an exponential cut-off at T_{cut}, so typically $T_X = 3-5\ \mathrm{keV}$.

[1] In Ref. [19], the curvature at the equator was calculated to be $\kappa R_A \approx 1.34$, still within the accuracy limit.

The solution to equation (15) reads as follows:

$$T = T_{\rm X} + (T_{\rm cr} - T_{\rm X}) \exp\left(-\frac{t}{t_{\rm C}}\right). \tag{17}$$

We note that $T_{\rm cr} \sim 30\,{\rm keV} \gg T_{\rm X} \sim 3\,{\rm keV}$. It is seen that the temperature decreases to $T_{\rm X}$ at $t \approx 2t_{\rm C}$. In the linear approximation, the temperature changes as

$$T \approx T_{\rm cr}\left(1 - \frac{t}{t_{\rm C}}\right). \tag{18}$$

Plugging this expression into formula (13), we find that the effective acceleration of gravity increases linearly with time as

$$g_{\rm eff} \approx \frac{GM}{R_{\rm A}^2}\,\frac{t}{t_{\rm C}}\cos\chi\,. \tag{19}$$

Correspondingly, the radial velocity of matter due to the instability growth increases with time as

$$u_{\rm r} = \int_0^{t_{\rm inst}} g_{\rm eff}\,{\rm d}t = \frac{GM}{R_{\rm A}^2}\,\frac{t_{\rm inst}^2}{2t_{\rm C}}\cos\chi\,. \tag{20}$$

Here, $t_{\rm indt}$ is the characteristic time of instability development, which can naturally be expressed in the form

$$t_{\rm inst} = \frac{K_0}{\omega_{\rm K}(R_{\rm A})}\,\frac{u_{\rm ff}}{u} = \frac{K_0}{\omega_{\rm K}(R_{\rm A}) f(u)}\,. \tag{21}$$

The choice of this expression is due to the fact that, in the case of rapid cooling, the velocity of matter $u_{\rm r}$ is on the order of the free-fall velocity $u_{\rm ff}$, and for slow cooling one has $u_{\rm r} \ll u_{\rm ff}$. We have also introduced the notation $f(u) \equiv u_{\rm r}/u_{\rm ff} < 1$, which will be used in what follows. K_0 is a dimensionless constant of the order of unity.

Plugging $t_{\rm indt}$ into formula (20), we find the velocity acquired by the matter during the timescale of the instability development:

$$u_{\rm r}(t_{\rm inst}) = \frac{K_0^2}{2}\,\frac{R_{\rm A}}{t_{\rm C} f^2(u)}\cos\chi\,. \tag{22}$$

Dividing both parts of this equation by $u_{\rm ff}$ and solving it for $f(u)$, we get the expression for $f(u)$:

$$f(u) = \left(\frac{K_0^2}{2}\right)^{1/3}\left(\frac{t_{\rm ff}}{t_{\rm C}}\right)^{1/3}(\cos\chi)^{1/3}\,. \tag{23}$$

Here, the expression for the free-fall time was used:

$$t_{\rm ff} \equiv \frac{R_{\rm A}}{u_{\rm ff}(R_{\rm A})} = \frac{R_{\rm A}^{3/2}}{\sqrt{2GM}}\,. \tag{24}$$

Then, the characteristic timescale for the instability can be rewritten in the form

$$t_{\rm inst} = \frac{(2K_0)^{1/3}}{\omega_{\rm K}(R_{\rm A})}\left(\frac{t_{\rm C}}{t_{\rm ff}}\right)^{1/3}(\cos\chi)^{-1/3}\,. \tag{25}$$

From this it follows that for $t_{\rm C} \gg t_{\rm ff}$ the timescale for the instability is much larger than the free-fall time:

$$\frac{t_{\rm inst}}{t_{\rm ff}} = 2^{1/2}(2K_0)^{1/3}\left(\frac{t_{\rm C}}{t_{\rm ff}}\right)^{1/3}(\cos\chi)^{-1/3}\,. \tag{26}$$

On the other hand, the timescale of the instability is shorter than the Compton cooling time:

$$\frac{t_{\rm inst}}{t_{\rm C}} = 2^{1/2}(2K_0)^{1/3}\left(\frac{t_{\rm ff}}{t_{\rm C}}\right)^{2/3}(\cos\chi)^{-1/3} < 1\,, \tag{27}$$

which allows us to utilize the linear expansion of temperature increase as a function of time (18).

The characteristic length of instability growth is defined as

$$\Delta = \int_0^{t_{\rm inst}} u_{\rm r}\,{\rm d}t = \frac{1}{6}\,\frac{GM}{R_{\rm A}^2}\,\frac{t_{\rm inst}^3}{t_{\rm C}}\cos\chi = \frac{1}{3}\,u_{\rm r} t_{\rm inst} = \frac{\sqrt{2}}{3}\,K_0 R_{\rm A}\,. \tag{28}$$

In this way, the scale of length of the instability becomes comparable to the magnetospheric radius during $t_{\rm indt}$, and the settling velocity turns out to be much smaller than the free-fall velocity $u_{\rm ff}$. It is apparent that late in the nonlinear stage of the instability growth the velocity of matter approaches the free-fall velocity.

We mainly consider the linear stage, since at this stage the plasma temperature is still high enough (although the entropy starts decreasing as the radius decreases), and it is in this zone that a toroidal component of the magnetic field is formed and effective angular momentum transfer from the magnetosphere to the shell takes place. At later stages of instability growth, the loss of entropy is too strong for convection to begin.

Let us estimate the accuracy of our approximation by retaining the second-order terms in the exponent expansion. Then, the velocity the matter acquired during the instability time $t_{\rm indt}$ is given by

$$u_{\rm r}(t_{\rm inst}) = K_0^{2/3}\left(\frac{GM}{t_{\rm C}}\right)^{1/3}(\cos\chi)^{1/3} \times\left[1 - \frac{2^{5/6}K_0^{1/3}}{3}\left(\frac{t_{\rm ff}}{t_{\rm C}}\right)^{2/3}(\cos\chi)^{-1/3}\right]. \tag{29}$$

Clearly, the smaller the accretion rate, the smaller the ratio $t_{\rm ff}/t_{\rm C}$, and the better our approximation.

Notice that for the magnetospheric radius in the form roughly defined by $\cos\lambda^n$, we have $\tan\chi = n\tan\lambda$. Therefore, for $n \simeq 0.27$ close to the equator, $\cos\chi \simeq 1$ with high accuracy, and in what follows we will ignore this factor. It should also be noted that $\cos\chi \simeq 0$ in the magnetospheric cusp region, and in this region matter can barely enter the magnetosphere at all.

Substituting formula (16) into Eqn (23) and then $f(u)$ into definition (11), we find at $\gamma = 5/3$ the expression for the Alfvén radius in this regime:

$$R_{\rm A} \approx 1.55\times 10^9 K_0^{2/11}\left[\left(1 + \frac{5}{3}\,m_{\rm t}^2\right)\psi\left(\frac{5}{3}\,, m_{\rm t}\right)\right]^{-3/11} \times\left(\frac{\mu_{30}^3}{\dot{M}_{16}}\right)^{2/11}[{\rm cm}]\,, \tag{30}$$

where $\mu_{30} \equiv \mu/(10^{30}\,{\rm G\,cm^3})$. We stress the difference between the expression just obtained for the Alfvén radius and the standard one, $R_{\rm A} \sim \mu^{4/7}/\dot{M}^{-2/7}$, which is derived by equating the dynamical pressure of free-falling gas to the magnetic field pressure; this difference comes from the dependence of $f(u)$ on the magnetic moment of a neutron star and mass accretion rate in the settling accretion regime.

The coefficient appeared due to turbulence, namely

$$K_{\rm t} = \left(1 + \frac{5}{3}\, m_{\rm t}^2\right) \psi\left(\frac{5}{3}\,,\, m_{\rm t}\right), \tag{31}$$

is obviously equal to 1 for isotropic turbulence [see expression (4) for ψ], and thus of interest only in the case of strong anisotropic turbulence.

Plugging expression (30) into Eqn (23), we arrive at an explicit expression for $f(u)$:

$$f(u) \approx 0.39 K_0^{7/11} K_{\rm t}^{1/22} \dot{M}_{16}^{4/11} \mu_{30}^{-1/11}\,. \tag{32}$$

A necessary condition for removal of angular momentum from the magnetosphere via convection in the shell is the condition of subsonic settling (the Mach number for the settling velocity equals $\mathcal{M} \equiv u_{\rm r}/u_{\rm s} < 1$), which for $\gamma = 5/3$ is reduced to the inequality $f(u) < 1/\sqrt{3}$. Clearly, this condition is fulfilled for mass accretion rates of around 10^{16} g s^{-1} and lower. It is also important to stress that convection in the shell, as well as the removal of angular momentum, practically stops working when the mean radial settling velocity $u_{\rm r}$ of the matter grows higher than the convective velocity $u_{\rm c}$, i.e., when the convective Mach number $m_{\rm c} = u_{\rm c}/c_{\rm s} \sim m_{\rm t}$ becomes smaller than the standard Mach number $\mathcal{M} = u_{\rm r}/c_{\rm s}$. And conversely, when the Mach number of the radial flow is smaller than the turbulent Mach number, $\mathcal{M} < m_{\rm t} \sim m_{\rm c}$, removal of angular momentum through the shell may take place.

When the rate of matter accretion through the shell gets larger than a certain critical value $\dot{M}^{\dagger}$ ($\dot{M} > \dot{M}^{\dagger}$), the velocity of the accretion flow close to the Alfvénic surface may become higher than the speed of sound, and a supersonic flow region with matter in free fall may form above the magnetosphere. It is not possible to withdraw any angular momentum from the rotating magnetosphere through this region. Therefore, settling accretion is not applicable here. A shockwave forms above the magnetosphere and plasma interaction with the magnetosphere is described in the scenario studied, for instance, in Ref. [10]. Depending on the inhomogeneity pattern in the captured stellar wind, the specific angular momentum of matter may be either positive or negative, and thus alternating episodes of spin-up and spin-down of the neutron star are possible in the supersonic regime. It is easy to estimate the critical X-ray luminosity above which the passage from the subsonic regime (at low X-ray luminosities) to the Bondi–Hoyle–Littleton accretion regime (at high X-ray luminosities) takes place. Indeed, assuming a limit for the dimensionless settling velocity equal to $f(u) = 0.5$ (at which removal of angular momentum through the shell is still possible; see Appendix E for details), we find from equation (32) the maximum possible value of the accretion rate for the settling regime with a removal of angular momentum:

$$\dot{M}_{16}^{\dagger} \approx 2 K_0^{-7/4} K_{\rm t}^{-1/8} \mu_{30}^{1/4}\,. \tag{33}$$

Notice that a similar value of the critical accretion rate can be found from a comparison of the Compton cooling time to the timescale for convection close to the Alfvén radius.

To conclude this section, we note that it is not difficult to perform a similar analysis for the velocity of matter entering to the magnetosphere due to radiative cooling of the plasma, for cases where Compton cooling is less effective [22]. This scenario may be realized in X-ray pulsars at very low accretion rates, when the shape of the X-ray beam-pattern changes and the photon beam forms a pencil diagram illuminating the magnetospheric cusp. In this way, one can explain the episodic 'off-states' (with very low X-ray luminosity), accompanied with a phase-shift in the X-ray pulse profile [23], as observed in pulsars like Vela X-1.

3. Transfer of angular momentum to the magnetosphere

Let us now highlight a quasistationary subsonic shell in which accretion proceeds onto the neutron star magnetosphere. We stress that in this regime, i.e., the settling regime, the accretion rate onto the neutron star is determined by the density at the bottom of the shell (which is directly related to the density downstream from the bow shock in the gravitational capture region) and the ability of the plasma to penetrate the magnetosphere through the Alfvénic surface.

The rotation law in the shell depends on the treatment of the turbulent viscosity (see Appendix B for cases where the Prandtl law and isotropic turbulence are applicable) and the possible anisotropy of the turbulence due to convection (see Appendix C). In the latter case, the anisotropy leads to more powerful radial turbulence compared with perpendicular one. In this way, as shown in Appendices B and C, we arrive at a set of quasipower-law solutions for the radial dependence of the angular rotation velocity in a convective shell. We shall consider in what follows a simple power-law dependence of the angular momentum on radius:

$$\omega(R) \sim R^{-n}\,. \tag{34}$$

In application to real pulsars we will use in Section 5 a quasi-Keplerian rotation law with $n = 3/2$, as well as an iso-angular momentum distribution with $n = 2$, which in some sense represent limiting cases among possible solutions.

When approaching the bow shock, $R \to R_{\rm B}$, the angular velocity of matter tend to the orbital velocity: $\omega \to \omega_{\rm B}$. Close to the bow shock, the problem is not spherically symmetric any more, since the flow becomes very complex (parts of the flow may cause the hot shell to bend, etc.), and the structure of the flow can only be studied using numerical simulations. In the absence of such simulations, we shall assume that the iso-angular-momentum distribution is established up to the bow shock front located at a distance from the neutron star which we shall take equal to the Bondi radius $R_{\rm B}$:

$$R_{\rm B} \simeq \frac{2GM}{V_{\rm w}^2 + v_{\rm orb}^2}\,,$$

where $V_{\rm w}$ is the stellar wind velocity at the neutron star orbital distance, and $v_{\rm orb}$ is the neutron star orbital velocity.

This means that the angular velocity $\omega_{\rm m}$ of rotation of matter near the magnetosphere will be related to $\omega_{\rm B}$ as follows:

$$\omega_{\rm m} = \tilde{\omega}\omega_{\rm B}\left(\frac{R_{\rm B}}{R_{\rm A}}\right)^n. \tag{35}$$

Here, the numerical factor $\tilde{\omega} > 1$ takes into account the deviation of the actual rotational law in the shell from the value obtained by using the assumed power-law dependence near the Alfvén radius (see Appendices B and C for more details).

Now, let the NS magnetosphere rotate with an angular velocity $\omega^* = 2\pi/P^*$, where P^* is the neutron star spin period. The matter at the bottom of the shell rotates with an angular velocity ω_m which is generally different from ω^*. If $\omega^* > \omega_m$, coupling of the plasma with the magnetosphere ensures transfer of angular momentum from the magnetosphere to the shell, or from the shell to the magnetosphere if $\omega^* < \omega_m$. In general, the coupling of matter with the magnetosphere can be either moderate or strong. In the strong coupling regime, the toroidal magnetic field component B_t is proportional to the poloidal field component B_p via the relation $B_t \sim -B_p(\omega_m - \omega^*)t$, and $|B_t|$ can grow up to $\sim |B_p|$. This regime can be realized in rapidly rotating magnetospheres, when ω^* is comparable to or even greater than the Keplerian angular frequency $\omega_K(R_A)$; in the latter case, the propeller regime sets in. In the moderate coupling regime, the plasma can enter into the magnetosphere due to the development of instabilities on a timescale shorter than the time needed for the toroidal field to grow to the value of the poloidal field, and thus $B_t < B_p$.

3.1 Strong coupling case

Let us first consider the strong coupling regime. In this regime, powerful large-scale convective motions of matter in the shell may lead to turbulent diffusion of a magnetic field accompanied by its dissipation. This process is characterized by the turbulent magnetic field diffusion coefficient η_t. In that case, the toroidal magnetic field (see, e.g., paper [5] and references cited therein) is written down in the form

$$B_t = \frac{R^2}{\eta_t}(\omega_m - \omega^*)B_p\,. \tag{36}$$

The turbulent magnetic diffusion coefficient is related to the kinematic turbulent viscosity as $\eta_t \simeq \nu_t$. The latter can be written down as

$$\nu_t = \langle u_t l_t \rangle\,. \tag{37}$$

According to the phenomenological Prandtl law, the average characteristics of a turbulent flow (the rate u_t, the characteristic spatial scale of turbulence l_t, and the shear $\omega_m - \omega^*$) are related in the following way:

$$u_t \simeq l_t|\omega_m - \omega^*|\,. \tag{38}$$

In our case, the turbulent scale must be determined by the largest scale of energy supply to the turbulence from the rotation of the nonspherical magnetospheric surface. This scale depends on the difference in velocity between the solidly rotating magnetosphere and the accreting matter that is still not interacting with the magnetosphere, namely $l_t \simeq R_A$, which determines the turnover velocity of the largest turbulence eddies. At smaller scales, a turbulent cascade develops. Substituting this scale into above equations (36)–(38), we find that $B_t \simeq B_p$ in the strong coupling regime.

The moment of forces due to plasma–magnetosphere interactions acts on the neutron star and changes its torque according to

$$I\dot{\omega}^* = \int \frac{B_t B_p}{4\pi}\,\varpi\,\mathrm{d}S = \pm\tilde{K}(\theta)K_2\,\frac{\mu^2}{R_A^3}\,, \tag{39}$$

where I is the neutron star's moment of inertia, ϖ is the distance from the rotational axis, and $\tilde{K}(\theta)$ is the numerical coefficient depending on the angle between the rotational and magnetic dipole axes. The coefficient K_2 appears in the above expression for the same reason as in formula (8). The positive sign in the right-hand side corresponds to a positive flux of angular momentum to the neutron star ($\omega_m > \omega^*$). The negative sign corresponds to a negative flux of angular momentum carried across the magnetosphere ($\omega_m < \omega^*$).

At the Alfvén radius, the matter couples with the magnetosphere and acquires the angular velocity of the neutron star. It then freely falls onto the neutron star surface and returns the angular momentum acquired at R_A back to the neutron star via the magnetic field. As a result of this process, the neutron star spins up at a rate determined by the expression

$$I\dot{\omega}^* = +z\dot{M}R_A^2\omega^*\,, \tag{40}$$

where z is the numerical coefficient which takes into account the mean specific angular momentum of the falling matter. If all the matter falls from the magnetosphere equator, then $z = 1$; if it falls strictly along the spin axis, then $z = 0$. If all the matter were to fall across the entire magnetospheric surface, then $z = 2/3$.

Ultimately, the total torque applied to the neutron star in the strong coupling regime changes its angular frequency according to the equation

$$I\dot{\omega}^* = \pm\tilde{K}(\theta)K_2\,\frac{\mu^2}{R_A^3} + z\dot{M}R_A^2\omega^*\,. \tag{41}$$

Using expression (11), we can eliminate $\dot{M}$ from the above equation to obtain in the spin-up regime ($\omega_m > \omega^*$):

$$I\dot{\omega}^* = \frac{\tilde{K}(\theta)K_2\,\mu^2}{R_A^3} \times\left[1 + z\,\frac{4\gamma f(u)}{\sqrt{2}(\gamma-1)(1+\gamma m_t^2)\,\psi(\gamma,m_t)\,\tilde{K}(\theta)}\left(\frac{R_A}{R_c}\right)^{3/2}\right], \tag{42}$$

where $R_c^3 = GM/\omega^{*2}$ is the corotation radius. In the spin-down regime ($\omega_m < \omega^*$), one finds

$$I\dot{\omega}^* = -\frac{\tilde{K}(\theta)K_2\,\mu^2}{R_A^3} \times\left[1 - z\,\frac{4\gamma f(u)}{\sqrt{2}(\gamma-1)(1+\gamma m_t^2)\,\psi(\gamma,m_t)\,\tilde{K}(\theta)}\left(\frac{R_A}{R_c}\right)^{3/2}\right]. \tag{43}$$

Notice that, in both cases, R_A must be smaller than R_c; otherwise, the propeller effect prohibits accretion. In the propeller regime, $R_A > R_c$, matter does not fall onto the neutron star, there are no accretion-generated X-rays from the neutron star, the shell rapidly cools down (see Section 6.1) and shrinks, and the standard Illarionov–Sunyaev propeller regime [15], with matter outflow from the magnetosphere, is established.

During both spin-up and spin-down, the neutron star angular velocity ω^* almost approaches the angular velocity of matter at the magnetospheric boundary: $\omega^* \to \omega_m(R_A)$. The difference between ω^* and ω_m is small, so the second term in the square brackets in equations (42) and (43) is much smaller than unity. Also note that when approaching the propeller regime ($R_A \to R_c$), the accretion rate decreases: $f(u) \to 0$, the second term in the square brackets vanishes, and the spin

evolution is determined solely by the spin-down moment of forces $-\tilde{K}(\theta)\mu^2/R_A^3$. [In the propeller regime, $\omega_m < \omega_K(R_A)$, $\omega_m < \omega^*$, and $\omega^* > \omega_K(R_A)$.] So, the neutron star spins down to the Keplerian frequency at the Alfvén radius. In that regime, the specific angular momentum of the matter flowing into and out from the magnetosphere is, of course, conserved.

Near equilibrium ($\omega^* \sim \omega_m$), relatively small fluctuations in $\dot{M}$ across the shell will lead to very strong fluctuations in $\dot{\omega}^*$, since the toroidal magnetic field component can change its sign by taking values from $+B_p$ to $-B_p$. If strong coupling actually occurs in nature, this property would be a distinguishing feature of this regime. It is well known (see, e.g., Refs [1, 24]) that actual X-ray pulsars sometimes exhibit rapid spin-up/spin-down transitions not associated with X-ray luminosity changes, which may be evidence that they temporarily enter the strong coupling regime. It cannot be ruled out that the triggering of the strong coupling regime may be due to the magnetic field frozen into the accreting plasma that has not yet entered the magnetosphere. Accretion of magnetized plasma onto neutron stars is studied in detail in the recent paper [25].

3.2 Moderate coupling case

The strong coupling regime considered above may be realized in the extreme case where the toroidal magnetic field B_t reaches its maximum possible value $\sim B_p$ due to magnetic turbulent diffusion. Usually, the coupling of matter with the magnetosphere is mediated by different plasma instabilities whose characteristic times are too short for substantial toroidal field growth. As discussed above in Section 2.1, the shell is very hot close to the magnetosphere boundary, so without cooling above it the plasma is marginally stable with respect to the interchange instability (according to the model calculations in Ref. [17]).

Let us write down the torque due to magnetic forces acting on the neutron star:

$$I\dot{\omega}^* = \int \frac{B_t B_p}{4\pi}\,\varpi\,\mathrm{d}S\,. \tag{44}$$

On the other hand, there is a mechanical torque applied to the magnetosphere from the base of the shell, caused by the turbulent stresses $W_{R\phi}$:

$$\int W_{R\phi}\varpi\,\mathrm{d}S\,, \tag{45}$$

where the viscous turbulent stresses can be written down as (see Appendix A for more details)

$$W_{R\phi} = \rho\nu_t R\,\frac{\partial\omega}{\partial R}\,. \tag{46}$$

Having specified the turbulent viscosity coefficient

$$\nu_t = \langle u_c l_t\rangle\,, \tag{47}$$

we assume that the characteristic scale of the turbulence close to the magnetosphere is $l_t \sim R_A$, and that the characteristic velocity of the turbulent pulsations is determined by the mechanism of eddy formation in the plasma above the magnetosphere. If there are strong convective motions in the shell caused by heating of its base, then $u_c \sim u_s$, where u_s is the speed of sound. If convection is prohibited, there is still turbulence caused by the shear flow in the shell ($\omega \sim 1/R^2$; see Appendix C). In this case, one finds $u_c(R_A) \sim u_\phi(R_A) \sim \omega^* R_A \ll u_s$. Obviously, the ratio between the stresses for the different cases turns out to be on the order of $\omega^*/\omega_K(R_A)$, which for slowly rotating pulsars is around 0.03–0.3. Equating torques (44) and (45), we get

$$\rho u_c R_A\,\frac{\partial\omega}{\partial R} = \frac{B_t B_p}{4\pi}\,. \tag{48}$$

We eliminate the density from this expression using the pressure balance at the magnetospheric boundary (8) and the expression for the temperature (4), and make the substitution

$$\frac{\partial\omega}{\partial R} = \frac{\omega_m - \omega^*}{\zeta R_A}\,. \tag{49}$$

Here, we have introduced the dimensionless factor $\zeta < 1$ characterizing the size of the zone in which an effective exchange of angular momentum between the magnetosphere and the base of the shell shows its worth. Hence follows the relation between the toroidal and poloidal components of the magnetic field in the magnetosphere:

$$\frac{B_t}{B_p} = \frac{\gamma}{\sqrt{2}(\gamma-1)K_t}\,\frac{u_c}{u_{ff}}\,\frac{\omega_m-\omega^*}{\zeta\omega_K(R_A)}\,. \tag{50}$$

Hereinafter, we use the following designations: the free fall velocity $u_{ff} \equiv \sqrt{2GM/R}$, the Keplerian frequency $\omega_K(R_A)$ at the magnetospheric boundary, and the correction coefficient $K_t \equiv (1+\gamma m_t^2)\,\psi(\gamma, m_t)$ due to turbulence. Substituting (50) into (44), in the case of convection $u_c = m_c u_s$ (where we have introduced the Mach number m_c for convective motions) we find that the spin-down rate of the neutron star is governed by the equation

$$I\dot{\omega}^* = \frac{K_1}{\zeta}\,K_2\,\frac{\mu^2}{R_A^3}\,\frac{\omega_m-\omega^*}{\omega_K(R_A)}\,, \tag{51}$$

where K_1 is a constant on the order of unity arising from a combination of the parameters in formula (50). In that case, formula (50) can be re-written in the form

$$\frac{B_t}{B_p} = \tilde{K}\,\frac{K_1}{\zeta}\,\frac{\omega_m-\omega^*}{\omega_K(R_A)}\,, \tag{52}$$

where the geometrical factors arising from the integration in Eqn (44) are included in the coefficient $\tilde{K} \sim 1$.

If the differential rotation at the base of the shell gives rise to turbulence, $u_c \sim u_\phi = \omega^* R_A$, then the expression for spin-down takes the form

$$I\dot{\omega}^* = \frac{\tilde{K}_1}{\zeta}\,K_2\,\frac{\mu^2}{R_A^3}\left(\frac{R_A}{R_c}\right)^{3/2}\frac{\omega_m-\omega^*}{\omega_K(R_A)}\,, \tag{53}$$

where

$$R_c \equiv \left(\frac{GM}{\omega^{*2}}\right)^{1/3} \tag{54}$$

is the corotational radius (see also paper [26]). Evidently, the braking torque turns out in this case to be smaller by a factor of $(R_A/R_c)^{3/2}$ than when there are convective motions in the shell. We will call this case *weak coupling*. It can easily be seen that in this case both the braking torque and the spin-down rate of the neutron star are independent of the mass accretion rate (in the limit $\omega_m \to 0$ we have just $K_{sd} \sim \mu^2/R_c^3$ [26]). As

will be discussed later in Section 5.3, the nonequilibrium pulsar GX 1 + 4 shows a negative correlation between $\dot{\omega}^*$ and luminosity during spin-down [27]. Therefore, we prefer braking according to law (51) (i.e., with moderate coupling).

Using the definition of the Alfvén radius R_A (11) and the expression for the Keplerian frequency ω_K, it is convenient to present formula (51) in the form

$$I\dot{\omega}^* = Z\dot{M}R_A^2(\omega_m - \omega^*)\,. \tag{55}$$

Here, the dimensionless coefficient Z was introduced:

$$Z = \frac{K_1/\zeta}{f(u)}\,\frac{\sqrt{2}(\gamma-1)}{4\gamma}\,K_t\,. \tag{56}$$

Substituting $\gamma = 5/3$ and expression (23) into this formula, we arrive at

$$Z \approx 0.363\,\frac{K_1}{\zeta}\,K_0^{-7/11}K_t^{21/22}\dot{M}_{16}^{-4/11}\mu_{30}^{1/11}\,. \tag{57}$$

Taking into account that the matter falling onto the neutron star brings in the angular momentum $z\dot{M}R_A^2\omega^*$ [see Eqn (40) above], we get

$$I\dot{\omega}^* = Z\dot{M}R_A^2(\omega_m - \omega^*) + z\dot{M}R_A^2\omega^*\,. \tag{58}$$

It is obvious that for angular momentum removal from the neutron star through such a shell, the coefficient Z has to be larger than z. Then, the accreting neutron star can episodically spin down (we will explain this statement in Section 4 in more details). And conversely, if $Z < z$, the neutron star can only spin up.

If a hot shell is not formed above the magnetosphere (at high X-ray luminosities or low-velocity stellar winds; see, e.g., Ref. [28] and Section 6.1), then the supersonic or Bondi accretion regime is established and no angular momentum can be removed from the neutron star. In this case, the equality $Z = z$ holds true, equation (58) takes the simple form $I\dot{\omega}^* = Z\dot{M}R_A^2\omega_m$, and the neutron star will spin up to a frequency on the order of $\omega_K(R_A)$ regardless of the sign of the difference $\omega_m - \omega^*$ between the angular velocities of the matter and the magnetic field lines close to the magnetospheric boundary. Due to conservation of the specific angular momentum, one obtains $\omega_m = \omega_B(R_B/R_A)^2$. Without the presence of a shell, the evolution of the angular frequency of the neutron star can thus be described by the equation

$$I\dot{\omega}^* = Z\dot{M}\omega_B R_B^2\,, \tag{59}$$

where the coefficient Z plays the role of the specific angular momentum of the matter captured. For example, $Z \simeq 1/4$ in the model of Ref. [15]. Numerical modeling of Bondi–Hoyle–Littleton accretion in two-dimensional (e.g., Refs [7, 29]) and three-dimensional (e.g., Refs [8, 9]) calculations have, however, shown that, due to inhomogeneities in the stellar wind, accretion occurs nonstationary and the sign of the captured angular momentum may change. The sign of Z may thus also be negative, and we may observe alternating spin-up and spin-down episodes. Such a scenario is often applied to explain the observed changes in the sign of the torques in accreting X-ray pulsars (see the discussion in paper [30]). We stress again that this picture may completely be realistic for X-ray pulsars at high luminosities exceeding 4×10^{36} erg s^{-1}, when, due to the strong Compton cooling around the rotating magnetosphere, no convective quasihydrostatic shell can be formed.

If a hot shell has indeed formed (at moderate X-ray luminosities less than $\sim 4 \times 10^{36}$ erg s^{-1} [see estimate (33)], the angular momentum from the neutron star magnetosphere can be transferred outside through the convective shell by means of turbulent viscosity. Therefore, substituting ω_m from formulas (35) and (58) yields

$$I\dot{\omega}^* = Z\dot{M}\tilde{\omega}\omega_B R_B^2\left(\frac{R_A}{R_B}\right)^{2-n} - Z\left(1 - \frac{z}{Z}\right)\dot{M}R_A^2\omega^*\,. \tag{60}$$

This is the basic formula that we will use later to describe the evolution of the spin of the neutron star.

The dimensionless coefficients in this relationship can be calculated using the factor $f(u)$, which is included in the expressions for Z and R_A. Thus, K_1/ζ is the only remaining dimensionless parameter in the model. In Section 5, we will show how this coefficient can be determined using observational data from real X-ray pulsars.

4. Spin-up and spin-down of X-ray pulsars

In this section, we will study the dependence of the accelerating and decelerating torques on the accretion rate $\dot{M}$. We would like to stress, again, that accretion in our case is subsonic, and the accretion rate is determined by the ability of matter to enter the magnetosphere through the shell. The velocity with which the plasma enters the magnetosphere is then mainly dependent on the density at the magnetospheric boundary. The density distribution in the shell, on the other hand, is directly connected to the density of matter in the shockwave region, and density variations downstream from the shock are thus rapidly translated into corresponding variations in the density near the magnetospheric boundary. This means that variations of the accretion rate onto neutron stars in binary systems with circular or low-eccentricity orbits should be essentially independent of the orbital phase, and be mostly determined by density variations in the stellar wind. In contrast, possible changes in the capture radius R_B (for example, due to velocity changes in the stellar wind or variations in the orbital velocity of the neutron star) have little effect on the accretion rate through the shell, but strongly affect the torques applied to the neutron star [see formula (60)].

Equation (60) can be rewritten in a form explicitly showing spin-up and spin-down torques:

$$I\dot{\omega}^* = A\dot{M}^{(2n+3)/11} - B\dot{M}^{3/11}\,. \tag{61}$$

For the characteristic value of the accretion rate $\dot{M}_{16} \equiv \dot{M}/(10^{16}\ \mathrm{g\ s^{-1}})$, the coefficients A and B (independent of the accretion rate) will be given (in CGS units) by

$$A \approx 4.22 \times 10^{31}(0.0388)^{2-n}\tilde{\omega}\,\frac{K_1}{\zeta}\,K_0^{-(2n+3)/11}K_t^{(9+6n)/22} \times \mu_{30}^{(13-6n)/11}\left(\frac{v_8}{\sqrt{\delta}}\right)^{-2n}\left(\frac{P_b}{10\ \mathrm{days}}\right)^{-1}, \tag{62}$$

$$B \approx 5.47 \times 10^{32}\left(1 - \frac{z}{Z}\right)\,\frac{K_1}{\zeta}\,K_0^{-3/11}K_t^{9/22}\mu_{30}^{13/11}\left(\frac{P^*}{100\ \mathrm{s}}\right)^{-1} \tag{63}$$

(from now on, we will assume $\gamma = 5/3$ in all numerical estimates). The dimensionless factor $\delta < 1$ takes into account the actual location of the gravitational capture

radius which for a cold stellar wind may be somewhat smaller than the Bondi radius [31]. The capture radius can also be reduced due to radiative heating of the stellar wind by the X-rays from the neutron star (see Section 6.1). To derive numerical values of the coefficients in formulas (62) and (63), we used expression (56) for the coefficient Z, and formulas (32) and (30) for the Alfvén radius.

In Sections 4.1 and 4.2, we will be concerned with the case of $Z - z > 0$, i.e., $B > 0$, since in the opposite case only spin-up of the neutron star is possible.

4.1 Equilibrium pulsars

For equilibrium pulsars, we set $\dot{\omega}^* = 0$, and from Eqn (58) we get

$$Z_{\rm eq}(\omega_{\rm m} - \omega^*) + z\omega^* = 0\,. \tag{64}$$

Close to equilibrium, we may vary equation (58) with respect to $\dot{M}$. It is convenient to introduce the dimensionless parameter $y \equiv \dot{M}/\dot{M}_{\rm eq}$, so that $y = 1$ close to equilibrium. Variations in $\delta\dot{M}$ may, in general, be caused by changes in density $\delta\rho$ and in the velocity δv of the stellar wind (and, thus, the Bondi radius). From the continuity equation and taking into account dependence (32) of $f(u)$ on $\dot{M}$ in the shell, we get

$$\frac{7}{11}\,\frac{\delta\dot{M}}{\dot{M}} = \frac{\delta\rho}{\rho} - 3\,\frac{\delta v}{v}\,. \tag{65}$$

Let us start by studying variations in the density only. Assuming $R_{\rm B} = {\rm const}$, we find

$$I\,\frac{\partial\dot{\omega}^*}{\partial\dot{M}}\bigg|_{\rm eq} = I\,\frac{1}{\dot{M}_{\rm eq}}\,\frac{\partial\dot{\omega}^*}{\partial y}\bigg|_{y=1} = \frac{4}{11}\,z\omega^* R_{\rm A}^2 + \frac{2n}{11}\,Z_{\rm eq}\omega_{\rm m} R_{\rm A}^2\,. \tag{66}$$

Using expression (64) for $\omega_{\rm m}$ and substituting it into equation (66) leads to

$$Z_{{\rm eq},\rho} - \frac{n-2}{n}\,z = \frac{I(\partial\dot{\omega}^*/\partial\dot{M})_{\rm eq}}{(2n/11)\omega^* R_{\rm A}^2} \approx \frac{3.64}{n}\left(\frac{(\partial\dot{\omega}^*/\partial y)_{y=1}}{10^{-12}}\right)\left(\frac{P^*}{100\ {\rm s}}\right) K_0^{-4/11} K_{\rm t}^{6/11}\dot{M}_{16}^{-7/11}\mu_{30}^{-12/11}\,. \tag{67}$$

Now, let us keep the density constant and study changes in the velocity only. Then, we have from equation (65) that $\delta v/v = -(7/33)\,\delta\dot{M}/\dot{M}$. Varying expression (58), we get

$$Z_{{\rm eq},v} - \frac{5n-3}{5n}\,z = \frac{I(\partial\dot{\omega}^*/\partial\dot{M})_{\rm eq}}{(20n/33)\omega^* R_{\rm A}^2} \approx \frac{1.1}{n}\left(\frac{(\partial\dot{\omega}^*/\partial y)_{y=1}}{10^{-12}}\right)\left(\frac{P^*}{100\ {\rm s}}\right) K_0^{-4/11} K_{\rm t}^{6/11}\dot{M}_{16}^{-7/11}\mu_{30}^{-12/11}\,. \tag{68}$$

A majority of neutron stars in X-ray pulsars rotate close to their equilibrium periods, at which, on average, $\dot{\omega}^* = 0$. Near equilibrium, in the settling accretion regime we get from equation (61):

$$\mu_{30}^{\rm eq} \approx \left(\frac{0.077\times(0.0388)^{2-n}\,\tilde{\omega}}{1 - z/Z}\right)^{11/(6n)} K_0^{-1/3} K_{\rm t}^{1/2}\left(\frac{\sqrt{\delta}}{v_8}\right)^{11/3} \times \dot{M}_{16}^{1/3}\left(\frac{P^*/100\ {\rm s}}{P_{\rm b}/10\ {\rm days}}\right)^{11/(6n)}\,. \tag{69}$$

This expression can be reversed to give the equilibrium spin period for a system if the magnetic field is known:

$$P_{\rm eq} \approx \frac{1300}{0.0388^{\,2-n}}\left(1 - \frac{z}{Z_{\rm eq}}\right)\tilde{\omega}^{-1} K_0^{2n/11} K_{\rm t}^{-3n/11}\mu_{30,{\rm eq}}^{6n/11} \times \left(\frac{P_{\rm b}}{10\ {\rm days}}\right)\dot{M}_{16}^{-2n/11}\left(\frac{v_8}{\sqrt{\delta}}\right)^{2n}\ [{\rm s}]\,, \tag{70}$$

where $v_8 \equiv v/(10^8\ {\rm cm\ s^{-1}})$. The ratio of the pulsar spin frequency to the Keplerian frequency at the Alfvén radius is independent of n:

$$\frac{\omega^*}{\omega_{\rm K}(R_{\rm A})} \approx 0.27 K_0^{3/11} K_{\rm t}^{-9/22}\left(\frac{P^*}{100\ {\rm s}}\right)^{-1}\mu_{30}^{9/11}\dot{M}_{16}^{-3/11}\,. \tag{71}$$

At equilibrium, the ratio between the toroidal and poloidal magnetic field components at the Alfvén radius [see Eqn (50)] takes the form

$$\frac{B_{\rm t}}{B_{\rm p}}\bigg|_{\rm eq} = -\frac{K_1}{\zeta}\,\frac{z}{Z_{\rm eq}}\,\frac{\omega^*}{\omega_{\rm K}(R_{\rm A})} = \frac{10 f(u) z}{\sqrt{2}K_{\rm t}}\,\frac{\omega^*}{\omega_{\rm K}(R_{\rm A})}\,. \tag{72}$$

Substituting $f(u)$ and ratio (71) into the last formula yields

$$\left|\frac{B_{\rm t}}{B_{\rm p}}\right|_{\rm eq} \approx 0.75 z\,\frac{K_0^{10/11}}{K_{\rm t}^{15/11}}\left(\frac{P^*}{100\ {\rm s}}\right)^{-1}\mu_{30}^{8/11}\dot{M}_{16}^{1/11}\,. \tag{73}$$

We stress that, for slowly rotating accreting pulsars, the ratio between the neutron star spin frequency and the Keplerian frequency at the Alfvén radius is always smaller than unity. Therefore, for typical values of $f(u) \sim 0.3$ and $z = 2/3$, we have $B_{\rm t}/B_{\rm p} < 1.5(\omega^*/\omega_{\rm K}(R_{\rm A})) < 1$, and the pulsars are far from being in the propeller regime (see further discussions in Section 6.2).

We would like to emphasize that in the important case of $n = 2$ (iso-angular-momentum distribution in the shell), the coefficient of the second term in formula (67) vanishes, and thus equating $Z_{\rm eq}$ to the right-hand side of Eqn (57) we find the magnetic moment of the neutron star expressed only in terms of the pulsar equilibrium period and the derivative $(\partial\dot{\omega}/\partial y)_{\rm eq}$:

$$\mu_{30,{\rm eq}} \approx 5\,\frac{(\partial\dot{\omega}^*/\partial y)_{y=1}}{10^{-12}}\,\frac{P^*}{100\ {\rm s}}\left(\frac{K_1}{\zeta}\right)^{-1} K_0^{3/11} K_{\rm t}^{-3/7}\dot{M}_{16}^{-3/11}\,. \tag{74}$$

For the case of $n = 2$ and a known $\mu_{\rm eq}$, we obtain the stellar wind velocity:

$$\frac{v_8}{\sqrt{\delta}} \approx 0.53\left(1 - \frac{z}{Z_{\rm eq}}\right)^{-1/4} K_0^{-1/11} K_{\rm t}^{3/22}\dot{M}_{16}^{1/11}\mu_{30,{\rm eq}}^{-3/11} \times \left(\frac{P^*/100\ {\rm s}}{P_{\rm b}/10\ {\rm days}}\right)^{1/4}\,. \tag{75}$$

As will be shown in Section 5, $z/Z_{\rm eq} \ll 1$ for real equilibrium pulsars, and thus the derived formula gives a correct estimate of the stellar wind velocity. Notice a weak dependence of the formula on the dimensionless constants and on the accretion rate. In the framework of our model, we may, thus, estimate the stellar wind velocity of the optical component without resorting to complicated spectroscopic measurements, if based on the measurements of the equilibrium spin period P^* and the binary period $P_{\rm b}$ and on the estimation of the neutron star magnetic field μ.

4.2 Nonequilibrium pulsars

First of all, it should be noted that the function $\dot{\omega}^*(\dot{M})$ reaches a minimum for some $\dot{M}_{\rm cr}$. Differentiating equation (61) with respect to $\dot{M}$ and equating the achieved expression to zero, one finds

$$\dot{M}_{\rm cr} = \left(\frac{B}{A}\,\frac{3}{3+2n}\right)^{11/(2n)} . \tag{76}$$

For $\dot{M} = \dot{M}_{\rm cr}$, the expression $\dot{\omega}^*$ reaches an absolute minimum (see Fig. 2).

It is convenient to introduce the dimensionless parameter

$$y \equiv \frac{\dot{M}}{\dot{M}_{\rm eq}} , \tag{77}$$

where $\dot{M}_{\rm eq}$ represents the accretion rate at which $\dot{\omega}^* = 0$:

$$\dot{M}_{\rm eq} = \left(\frac{B}{A}\right)^{11/(2n)} . \tag{78}$$

It is evident that

$$\dot{M}_{\rm cr} = \dot{M}_{\rm eq}\left(\frac{3}{2n+3}\right)^{11/(2n)} , \tag{79}$$

in other words, $\dot{\omega}^*$ goes through a minimum at following values of the dimensionless parameter

$$y_{\rm cr} = \left(\frac{3}{2n+3}\right)^{11/(2n)} < 1 . \tag{80}$$

Equation (61) can be rewritten in the form

$$I\dot{\omega}^* = A\dot{M}_{\rm eq}^{(3+2n)/11} y^{(3+2n)/11}\left(1 - y^{-2n/11}\right) . \tag{81}$$

The minimum of $\dot{\omega}^*$ at $y = y_{\rm cr}$ (i.e., the maximum possible spin-down rate of the pulsar) is defined as

$$I\dot{\omega}^*_{\rm min} = -\frac{2n}{3}\,A\dot{M}_{\rm eq}^{(3+2n)/11} y^{(3+2n)/11} . \tag{82}$$

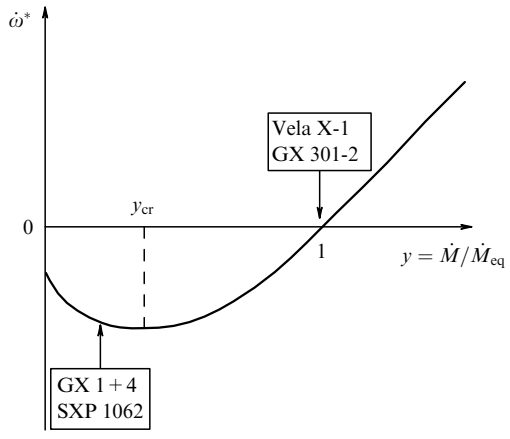

Figure 2. An illustration of the dependence of $\dot{\omega}^*$ on the dimensionless accretion rate t [see formula (81)]. In fact, as $y \to 0$, $\dot{\omega}^*$ approaches some negative value, since the neutron star enters the propeller regime at small accretion rates. The figure shows the position in the diagram for equilibrium pulsars with $y \approx 1$, and for nonequilibrium pulsars at steady spin-down with $y < y_{\rm cr}$.

Now, we vary equation (81) with respect to y:

$$I\delta\dot{\omega}^* = I\,\frac{\partial\dot{\omega}^*}{\partial y}\,\delta y = \frac{3}{11}\,A\dot{M}_{\rm eq}^{(3+2n)/11} y^{-8/11} \times \left(\frac{2n+3}{3}\,y^{2n/11} - 1\right)\delta y . \tag{83}$$

Apparently, depending on whether $y > y_{\rm cr}$ or $y < y_{\rm cr}$ is fulfilled, *correlated changes* in $\delta\dot{\omega}^*$ with X-ray flux should have different signs. Indeed, a positive correlation between the observed δP^* and $\delta\dot{M}$ was found for GX 1+4 using CGRO BATSE and Fermi gamma-ray burst monitor (GBM) data [27, 32]. This means that there is a negative correlation between $\delta\omega^*$ and $\delta\dot{M}$ in this pulsar, suggesting $y < y_{\rm cr}$ in this source.

Let us now consider accreting pulsars (GX 1+4, SXP 1062, etc.) in the stage of spin-down. If the pulsar is spinning down, measurements of the spin-down rate put limits on the parameters of our model. From the simple fact that the spin-down is stable, we may obtain using equations (61)–(63) a lower limit on the NS magnetic field in the case of quasispherical accretion with $\dot{\omega}^* < 0$:

$$\mu_{30} > \mu_{30,\rm min} \approx 0.1\left(1 - \frac{z}{Z}\right)^{-11/12} \tilde{\omega}^{11/12} K_0^{-1/3} K_{\rm t}^{1/2} \times \left(\frac{\sqrt{\delta}}{v_8}\right)^{11/3} \dot{M}_{16}^{1/3}\left(\frac{P^*/100\ {\rm s}}{P_{\rm b}/10\ {\rm days}}\right)^{11/12} \tag{84}$$

[thus, equation (69) was transformed here into an inequality]. We now make use of the fact that during spin-down there is a maximum possible braking torque [see Eqn (82)]. Inserting the values of the coefficients A and B from equations (62) and (63) into formula (82), we find

$$\dot{\omega}^*_{\rm sd,\,max} \approx -1.13\times 10^{-12}\left(1 - \frac{z}{Z}\right)^{7/4} \frac{K_1}{\zeta}\,\mu_{30}^2\left(\frac{v_8}{\sqrt{\delta}}\right)^3 \times \left(\frac{P^*}{100\ {\rm s}}\right)^{-7/4}\left(\frac{P_{\rm b}}{10\ {\rm days}}\right)^{3/4} [{\rm rad\ s^{-2}}] . \tag{85}$$

The maximum braking torque is reached at the accretion rate $\dot{M} = \dot{M}_{\rm cr}$:

$$\dot{M}_{16,\,\rm cr} \approx 112\left(1 - \frac{z}{Z}\right)^{11/4} K_0 K_{\rm t}^{-2} \mu_{30}^3\left(\frac{v_8}{\sqrt{\delta}}\right)^{11}\left(\frac{P_{\rm b}/10\ {\rm days}}{P^*/100\ {\rm s}}\right)^{11/4} \tag{86}$$

(notice here the extremely strong dependence of this estimate on the stellar wind velocity). Then, from the condition $|\dot{\omega}^*_{\rm sd}| \leqslant |\dot{\omega}^*_{\rm sd,\,max}|$ follows a more interesting lower limit on the neutron star magnetic field:

$$\mu_{30} > \mu'_{30,\,\rm min} \approx 0.94\left|\frac{\dot{\omega}^*_{\rm sd}}{10^{-12}\ {\rm rad\ s^{-2}}}\right|\left(\frac{K_1}{\zeta}\right)^{-1/2}\left(\frac{v_8}{\sqrt{\delta}}\right)^{-3/2} \times \left(\frac{P^*}{100\ {\rm s}}\right)^{7/8}\left(\frac{P_{\rm b}}{10\ {\rm days}}\right)^{-3/8} . \tag{87}$$

Of concern to us is the weaker dependence of this estimate on the stellar wind velocity compared to the estimate determined by inequality (84).

If the accelerating torque can be neglected, in contrast to the braking torque (corresponding to the low X-ray luminosity limit of $y \ll 1$), then it directly follows from formula (51)

that the spin-down rate for accreting pulsars equals

$$\dot{\omega}^*_{\rm sd} \approx -0.55\times10^{-12}\,\frac{K_1}{\zeta}\,K_0^{-3/11}K_{\rm t}^{9/22}\mu_{30}^{13/11}\dot{M}_{16}^{3/11} \times\left(\frac{P^*}{100\ {\rm s}}\right)^{-1}\ [{\rm rad\ s^{-2}}]\,. \quad (88)$$

From this relationship we obtain a lower limit on the neutron star magnetic field that neither depends on the parameters of the stellar wind nor on the binary orbital period:

$$\mu_{30} > \mu''_{30,\min} \approx 1.66\left|\frac{\dot{\omega}^*_{\rm sd}}{10^{-12}\ {\rm rad\ s^{-2}}}\right|^{11/13}\left(\frac{K_1}{\zeta}\right)^{-11/13} \times K_0^{3/13}K_{\rm t}^{-9/26}\dot{M}_{16}^{-3/13}\left(\frac{P^*}{100\ {\rm s}}\right)^{11/13}. \quad (89)$$

Eliminating K_1/ζ from formulas (51) and (52), we arrive at

$$\left|\frac{B_{\rm t}}{B_{\rm p}}\right| = \tilde{K}\left|\frac{I\dot{\omega}^*_{\rm sd}R_{\rm A}^3}{K_2\,\mu^2}\right| \approx 0.49\left|\frac{\dot{\omega}^*_{\rm sd}}{10^{-12}\ {\rm rad\ s^{-2}}}\right|\mu_{30}^{-4/11}K_0^{6/11}K_{\rm t}^{-9/11}\dot{M}_{16}^{-6/11}\,. \quad (90)$$

It is seen from the last formula that with decreasing $\dot{M}$ the ratio $B_{\rm t}/B_{\rm p}$ increases for reasons well understood — the characteristic cooling time for the plasma increases at low $\dot{M}$ and the toroidal component has time to grow to the same strength as the poloidal. However, $B_{\rm t}$ cannot become larger than $B_{\rm p}$ due to developing an instability similar to that of a tightly wound spring. Equating $B_{\rm t} = B_{\rm p}$, we find from formula (90) the luminosity value below which the pulsar enters the strong coupling regime during spin-down (see Section 3.1):

$$\dot{M}^*_{16} \approx 0.27\left|\frac{\dot{\omega}^*_{\rm sd}}{10^{-12}\ {\rm rad\ s^{-2}}}\right|^{11/6}\mu_{30}^{-2/3}K_0K_{\rm t}^{-3/2}\,. \quad (91)$$

Below this luminosity level in the strong coupling regime, the spin-down law becomes $K_{\rm sd} \sim \mu^2R_{\rm A}^{-3} \sim \dot{M}^{6/11}$:

$$\dot{\omega}^*_{\rm sd} \approx -2\times10^{-12}\,\mu_{30}^{4/11}K_0^{-6/11}K_{\rm t}^{9/11}\dot{M}_{16}^{6/11}\ [{\rm rad\ s^{-2}}]\,. \quad (92)$$

(Notice that when the spin-up torque can be neglected, the expression does not contain the ever-so-hard-to-determine velocity of the stellar wind.)

For a further decrease in the accretion rate in non-equilibrium pulsars, the Alfvén radius will grow to the corotation radius, and the pulsar may enter a transient state (the propeller regime). From the condition $\omega^* = (GM/R_{\rm A}^3)^{1/2}$, we find the accretion rate for this transition:

$$\dot{M}^{**}_{16} \approx 0.0082K_0K_{\rm t}^{-3/2}\mu_{30}^3\left(\frac{P^*}{100\ {\rm s}}\right)^{-11/3}. \quad (93)$$

The formulas derived above show that the restrictions on the model become more significant if the neutron star magnetic field can be measured independently (for example, utilizing spectral cyclotron lines). We also would like to stress the fact that measurements of correlated fluctuations of the spin frequency derivative with luminosity during spin down (similar to the analysis presented in Section 5.3 for GX 1 + 4) allow us to place the source in a $\dot{\omega}^* - y$ diagram (see Fig. 2). To the right of the minimum, $y > y_{\rm cr}$ and the correlation is positive. To the left, $y < y_{\rm cr}$ and the correlation is negative. In this way, we may obtain further limits on the parameters of our model.

5. Application to real X-ray pulsars

In this section, as an illustration of the possible applicability of our model to real sources, we will consider five particular slowly rotating moderately luminous X-ray pulsars: GX 301-2, Vela X-1, GX 1 + 4, SXP 1062, and 4U 2204 + 56.

The first two pulsars have spin periods close to those for the equilibrium rotation of the neutron star, showing spin-up/spin-down excursions near the equilibrium frequency (apart from the spin-up/spin-down jumps, which may be, we believe, due to episodic switch-ons of the strong coupling regime when the toroidal magnetic field component becomes comparable to the poloidal one; see Section 3.1).

The third source, GX 1 + 4, is a typical example of a pulsar displaying long-term spin-up/spin-down episodes. During the last 30 years, it has shown a steady spin-down with frequency derivative fluctuations anticorrelated with X-ray luminosity (see paper [32] for a more detailed discussion). Clearly, this pulsar cannot be considered in equilibrium.

The pulsar SXP 1062 in the Large Magellanic Cloud and the pulsar 4U 2206 + 54 have only been observed at steady spin-down.

5.1 GX 301-2

GX 301-2 (also known as 4U 1223-62) is a high-mass X-ray binary consisting of a neutron star and an early type B optical companion with mass $\simeq 40M_\odot$ and radius $\simeq 60R_\odot$. The binary period covers 41.5 days [33]. The neutron star is a $\approx$ 680-s X-ray pulsar [34] accreting from the strong wind of its companion ($\dot{M}_{\rm loss} \sim 10^{-5}M_\odot$/yr [35]). The photospheric escape velocity of the wind is $v_{\rm esc} \approx 500$ km s^{-1}. The semi-major axis a of the binary system measures approximately $170R_\odot$, and the orbital eccentricity $e \approx 0.46$. The wind terminal velocity was found to be about 300 km s^{-1} [35], smaller than the photospheric escape velocity.

GX 301-2 exhibits strong short-term pulse period variability, which, as in many other wind-accreting pulsars, can be well described by a random walk model [36]. Earlier observations between 1975 and 1984 revealed a pulse period of $\approx$ 700 s, while in 1984 the source started to spin up [37]. The almost 10 years of spin-up were followed by a reversal of spin in 1993 [38], after which the source has been continuously spinning down [39–41]. Rapid spin-up episodes sometimes appear in the Fermi GBM data on top of the long-term spin-down trend [24]. It cannot be ruled out that these rapid spin-up episodes, as well as similar ones observed in burst and transient source experiment (BATSE) data, reflect a temporary entrance into the strong coupling regime, as discussed in Section 3.1. Cyclotron line measurements [39] yield a magnetic field estimate near the neutron star surface of $B_0 \approx (5.1-5.8)\times10^{12}$ G ($\mu = 1/2B_0R_0^3 = (2.6-2.9)\times10^{30}$ G cm^3 for the assumed neutron star radius $R_0 = 10$ km).

In Fig. 3 we have plotted the observed frequency derivative $\dot{\omega}^*$ as a function of the observed pulsed X-ray flux (20–40 keV) according to BATSE data (see Ref. [41] for more detail). We will consider the neutron star magnetic field in this source to be known from observations. An estimate of $\dot{M}$ can be inferred from the X-ray flux, provided the distance to the source is known, which is generally not the case to a great certainty. We shall assume that near equilibrium a hot

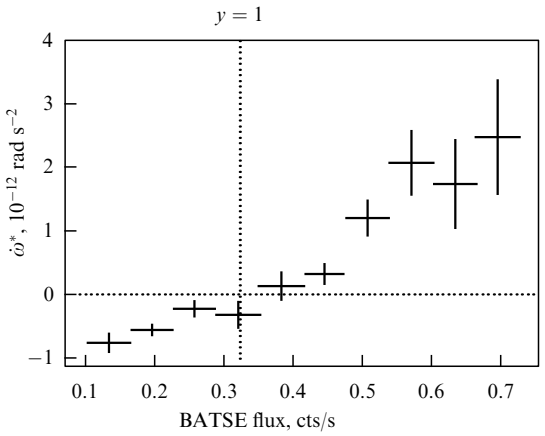

Figure 3. Torque–luminosity correlation in GX 301-2: $\dot{\omega}^*$ as a function of BATSE data (20–40 keV pulsed flux) near the equilibrium frequency (see Ref. [41]). The assumed X-ray flux at equilibrium (in terms of the dimensionless parameter y) is also shown by the vertical dotted line.

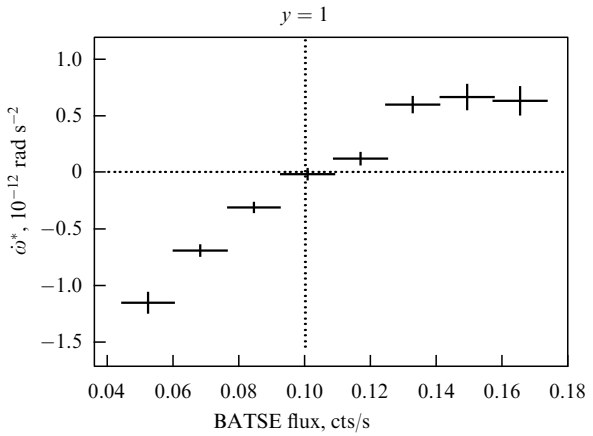

Figure 4. The same as in Fig. 3 for Vela X-1 [55].

quasispherical shell exists in this pulsar, and that the accretion rate is of order 3×10^{16} g s^{-1}, i.e., not higher than the critical value of $\dot{M}_*^{\dagger} \simeq 4 \times 10^{16}$ g s^{-1} [see formula (33)]. The derivative $\partial\dot{\omega}^*/\partial y$ can be obtained from the $\dot{\omega}^*$–X-ray flux plot, since the accretion rate in the first approximation is proportional to the observed pulsed X-ray flux. Near equilibrium (the torque reversal point $y = 1$ with $\dot{\omega}^* = 0$), we find from a linear fit in Fig. 3 that $\partial\dot{\omega}^*/\partial y \approx 1.5 \times 10^{-12}$ rad s^{-2}.

The obtained parameters (Z, K_1/ζ, etc.) for this pulsar are listed in Table 1. It is seen that the toroidal component of the magnetic field is much less than the poloidal (the pulsar resides far from the strong-coupling limit). The stellar wind velocity determined by formula (75) is close to the photospheric escape velocity. We also note that the value of the parameter K_1/ζ describing the coupling between the plasma and the magnetosphere is on the order of 14, although by its physical sense the coefficient K_1 should be on the order of 1. This means that the value of the parameter ζ, which gives the characteristic relative size of the region in which the transfer of angular momentum from the shell to the magnetosphere takes place (or vice versa), has to be around 1/10 (i.e., the characteristic size of the region where angular momentum transfer takes place should be approximately 1/10 of the Alfvén radius).

5.2 Vela X-1

Vela X-1 (≡4U 0900-40) constitutes the brightest persistent accretion-powered pulsar in the 20–50 keV energy range, with

Table 1. Parameters of the discussed pulsars.†

	Equilibrium pulsars		Nonequilibrium pulsars		
	GX 301-2	Vela X-1	GX 1+4	SXP 1062	4U 2206+54
	Measured parameters				
P^*, s	680	283	140	1062	5560
P_b, day	41.5	8.96	1161	∼ 300‡	19
v_w, km s^{-1}	300	700	200	∼ 300§	350
μ_{30}	2.7	1.2	?	?	1.7
$\dot{M}_{16}$	3	3	1	0.6	0.2
$(\partial\dot{\omega}/\partial y)_{y=1}$, rad s^{-2}	1.5×10^{-12}	1.2×10^{-12}	—	—	—
$\dot{\omega}^*_{sd}$, rad s^{-2}	0	0	-2.34×10^{-11}	-1.63×10^{-11}	-9.4×10^{-14}
	Calculated parameters¶				
$f(u)$	0.53	0.57			
K_1/ζ	14	10			$\gtrsim 8$
Z	3.7	2.6			
B_t/B_p	0.17	0.22			
R_A, cm	2×10^9	1.4×10^9			
$\omega^*/\omega_K(R_A)$	0.07	0.08			
$v_{w,min}$, km s^{-1}	500	740			
$\mu_{30,min}$			$\mu'_{min} \approx 4$	$\mu''_{min} \approx 20$	$\mu'_{min} \approx 3.6$

† References for the observed pulsar and orbital parameters, as well as values for the wind velocities from measurements of the optical components, are given in Section 5. The dimensionless parameters Z, K_1/ζ, and $f(u)$ were derived in Sections 2.3 and 3.
‡ Estimate from the source's position in the Corbet $P^* - P_b$ diagram.
§ Estimate of typical wind velocity in binary pulsars containing Be-stars.
¶ Numerical estimates are given assuming iso-angular-momentum rotation in the shell ($n = 2$), moderate coupling between the plasma and the magnetic field, and values of dimensionless parameters $\delta = 1$, $\zeta = 1$, $\tilde{\omega} = 1$, $K_0 = 1$, $\gamma = 5/3$ in the absence of turbulence in the shell ($m_t = 0$, $K_t = 1$).

an average luminosity of $L_X \approx 4 \times 10^{36}$ erg s^{-1} [37]. It consists of a massive neutron star (1.88 $M_\odot$ [42]) and the B0.5Ib super giant HD 77581, which eclipses the neutron star every orbital cycle of ~ 8.964 days [43]. The neutron star was discovered as an X-ray pulsar with a spin period of ≈ 283 s [44], which has remained almost constant since the discovery of the source. The optical companion has a mass and radius of $\approx 23 M_\odot$ and $\approx 30 R_\odot$, respectively [43]. The photospheric escape velocity is $v_{esc} \approx 540$ km s^{-1}. The orbital separation is $a \approx 50 R_\odot$, and the orbital eccentricity $e \approx 0.1$. The primary almost fills its Roche lobe (as also evidenced by the presence of elliptical variations in the optical light curve [45]. The mass-loss rate from the primary star runs to $10^{-6} M_\odot$ yr^{-1} [46] via a fast wind with a terminal velocity of ~ 1100 km s^{-1} [47], which is typical for this spectral class. Despite the fact that the terminal velocity of the wind is rather large, the compactness of the system makes it impossible for the wind to reach this velocity before interacting with the neutron star, so the relative velocity of the wind with respect to the neutron star is rather low, namely ~ 700 km s^{-1}.

Cyclotron line measurements [48] yield the magnetic field estimate $B_0 \approx 3 \times 10^{12}$ G ($\mu = 1.5 \times 10^{30}$ G cm^3 for the assumed neutron star radius of 10 km). We shall assume that in this pulsar $\dot{M} \simeq 3 \times 10^{16}$ g s^{-1} (again, for the existence of a shell to be possible).

In Fig. 4, we have plotted $\dot{\omega}^*$ as a function of the observed pulsed X-ray flux (20–40 keV) according to BATSE data [49]. As in the case of GX 301-2, from a linear fit we find at the spin-up/spin-down transition point that $\partial\dot{\omega}^*/\partial y \approx 1.2 \times 10^{-12}$ rad s^{-2}.

The parameters obtained for Vela X-1 are listed in Table 1. We note that the velocity of the stellar wind as found using formula (75) is very close to the observed value of 700 km s^{-1}. As in the case of GX 301-2, the value of the coupling parameter K_1/ζ is on the order of 10, i.e., the size of the region for transfer of angular momentum between the plasma and the magnetosphere comes to about 1/10 of the Alfvén radius.

5.3 GX 1+4

GX 1+4 was the first source to be identified as a symbiotic binary containing a neutron star [50]. The pulse period covers ~ 140 s, and the donor is an MIII giant [50]. The system has an orbital period of 1161 days [51], making it the widest known LMXB with the period exceeding the typical one by at least an order of magnitude. The donor is far from filling its Roche lobe, and accretion onto the neutron star proceeds by capturing the stellar wind of the companion.

The system has a very interesting NS spin history. During the 1970s, it was spinning up at the fastest rate ($\dot{\omega}_{su} \sim 3.8 \times 10^{-11}$ rad s^{-2}) among the known X-ray pulsars at the time (see, e.g., Ref. [37]). After several years of nondetection in the early 1980s, it reappeared with an increased spin period, now spinning down at a rate similar in magnitude to that of the previous spin-up. At present, the source is steadily spinning down with an average spin-down rate of $\dot{\omega}^*_{sd} \approx -2.34 \times 10^{-11}$ rad s^{-2}. The observed spin-reversal has been interpreted in terms of a retrograde accretion disc being formed in the system from a stellar wind [27, 52, 53]. A detailed spin-down history of the source is discussed in the recent paper [32]. Using our model, this behavior can, however, be readily explained in the framework of quasispherical accretion.

As the GX 1+4 pulsar is not in equilibrium, we may apply one of the three formulas from Section 4.2 to derive a lower limit on the neutron star magnetic field from the observed value of $\dot{\omega}_{sd}$. From formula (87) we get $\mu'_{30,\,min} \approx 12(K_1/\zeta)^{-1/2}$. Assuming that the coupling parameter for nonequilibrium pulsars is similar to that in equilibrium ones (and, thus, that the size of the region where the transfer of angular momentum between the plasma and the magnetosphere takes place is on the order of 1/10 of the Alfvén radius: $\zeta \sim 0.1$), we find that $\mu'_{30,\,min} \sim 4$.

In this source, one can also observe anticorrelated variability in spin-down rate versus X-ray luminosity [27]. According to the latest Fermi GBM data in paper [32], it was found that $-\dot{\omega}^* \sim L_X^{0.3}$. Our model for moderate coupling yields $K_{sd} \sim \dot{M}^{3/11}$, which is very similar to the observed relation. It was found in the earlier BATSE observations [27] that $-\dot{\omega}^* \sim L_X^{0.48}$. It cannot be ruled out that the average luminosity of the source was somewhat lower at that time. In this case, component B_t could have been closer to B_p, and then the expected correlation would have had the form $K_{sd} \sim \dot{M}^{6/11} \sim L_X^{0.54}$. Note that in the model with a weak coupling (with the transfer of angular momentum due to turbulence close to the magnetosphere [26]), the braking torque is less effective by a factor of $(R_A/R_c)^{3/2}$ and not at all dependent on the luminosity. In low-luminosity pulsars, the cooling close to the Alfvén radius is less effective, thus leading to the development of convective motions in the shell and the establishment of the moderate coupling regime.

Further, we note that the short-term spin-up episodes, sometimes observed on top of the steady spin-down behavior (at about MJD 49700; see Fig. 2 in paper [27]), are correlated with an enhancement of the X-ray flux, in contrast to the negative frequency–flux correlations discussed above. During these short spin-ups, the frequency derivative $\dot{\omega}^*$ is about half the average $\dot{\omega}^*_{su}$ observed during the steady spin-up state of NS in GX 1+4 up to 1980. The X-ray luminosity during these episodic spin-ups was approximately five times larger than the mean X-ray luminosity during the steady spin-down. We remind the reader that once $\dot{M} > \dot{M}^\dagger$, a free-fall gap appears above the magnetosphere, and the neutron star can only spin up. When the X-ray flux drops again, the subsonic settling regime is re-established and the neutron star resumes its spin-down.

5.4 SXP 1062

This recently discovered young X-ray pulsar resides in a Be/X-ray binary system located in a supernova remnant in the Small Magellanic Cloud. Its rotational period is $P^* \approx 1062$ s, and it has a low X-ray luminosity of $L_X \approx 6 \times 10^{35}$ erg s^{-1} [54]. The source exhibits a remarkably high spin-down rate of $\dot{\omega}^* \approx -1.6 \times 10^{-11}$ rad s^{-2}. Its origin is widely discussed in the literature (see, e.g., Refs [55, 56]), and a possible presence of anomalously high magnetic field in the neutron star has been suggested [57]. In the framework of our model, we take advantage of more conservative limits. Neglecting the spin-up torque (89), we get $\mu_{30} > \mu''_{30,\,min} \approx 20$. This implies that the observed spin-down can be explained by a magnetic field on the order of 10^{13} G, and thus we believe it is premature to conclude that the source is an accreting magnetar.

5.5 4U 2204+54

This slowly rotating pulsar has a spin period of $P^* = 5560$ s and exhibits a spin-down rate of $\dot{\omega}_{sd} \approx -9.4 \times 10^{-14}$ rad s^{-2}

[58]. The orbital period P_b of the binary system covers about 19 days [58], and the measured stellar wind velocity v_w reaches approximately 350 km s^{-1}, which is abnormally low for an O9.5V optical counterpart [59]. The X-ray luminosity of the source equals, on average, $L_X \simeq 2\times10^{35}$ erg s^{-1}. A feature in the X-ray spectrum sometimes observed around 30 keV can be interpreted as a cyclotron line [60–63]. That gives an estimate of the magnetic field approaching approximately $B \sim (30/11.6)\times1.3\times10^{12} \approx 3.4\times10^{12}$ G (taking into account the gravitational redshift close to the surface: $1+z\sim1.3$), and thus $\mu_{30}\approx1.7$. Utilizing this value of the magnetic field and neglecting the accelerating torque, from formula (88) we obtain a lower limit on the parameter $K_1/\zeta \gtrsim 8$, which is very close to the coupling parameter values for the equilibrium Vela X-1 and GX 301-2 pulsars. If we consider the NS magnetic field to be unknown (see the discussion in paper [58]) and apply formula (87), as in the case of GX 1+4, then assuming moderate coupling with $K_1/\zeta\sim10$, we get the limit $\mu_{30} > \mu'_{30,\,\min}\approx3.6$, which is in agreement with standard neutron star magnetic field values. Notice that recklessly applying our formulas to equilibrium pulsars here would give a magnetar value for the magnetic field [58].

6. Discussion

6.1 Physical conditions inside the shell

For an accretion shell to be formed around the neutron star magnetosphere, it is necessary that the matter crossing the bow shock not cool down too rapidly, and thus not start to fall freely. This means that the radiation cooling time t_{cool} must be longer than the characteristic time of plasma falling.

The plasma is heated up behind the strong shock to a temperature

$$T_{ps} = \frac{3}{16}\,\mu_m\,\frac{v_w^2}{\mathcal{R}} \approx 1.36\times10^5\left(\frac{v_w}{100\text{ km s}^{-1}}\right)^2\text{ [K]}. \quad (94)$$

The radiative cooling time of the plasma is defined as

$$t_{cool} = \frac{3kT}{2\mu_m n_e \Lambda}, \quad (95)$$

where ρ is the plasma density, $n_e = Y_e\rho/m_p$ is the electron number density (molecular weight $\mu_m = 0.6$ and lepton number $Y_e\approx0.8$ for fully ionized plasma with solar abundance), and Λ is the cooling function which can be approximated as [64, 65]

$$\Lambda(T) = \begin{cases} 0, & T < 10^4\text{ K},\\ 1.0\times10^{-24}T^{0.55}, & 10^4 < T < 10^5\text{ K},\\ 6.2\times10^{-19}T^{-0.6}, & 10^5 < T < 4\times10^7\text{ K},\\ 2.5\times10^{-27}T^{0.5}, & T > 4\times10^7\text{ K}. \end{cases} \quad (96)$$

Compton cooling becomes effective from the radius R_X where the gas temperature T, determined by the hydrostatic formula (4), is lower than the Compton X-ray temperature T_X. The Compton cooling time [see formula (16)] is given by

$$t_C \approx 1060\dot{M}_{16}^{-1}\left(\frac{R}{10^{10}\text{ cm}}\right)^2\text{ [s]}. \quad (97)$$

Above the radius where $T_X = T$, Compton heating dominates. Taking the actual temperature close to the adiabatic one (4), we find $R_X\approx2\times10^{10}$ cm. It should be noted that both the Compton and photoionization heating processes are controlled by the photoionization parameter ξ [66, 67]:

$$\xi = \frac{L_X}{n_e R^2}. \quad (98)$$

In most part of the accretion flux, the density distribution follows $n\sim R^{-3/2}$, so $\xi\sim R^{-1/2}$ and is independent of the X-ray luminosity if the mass continuity equation is taken into account. We derive a characteristic value for ξ:

$$\xi \approx 5\times10^5 f(u) R_{10}^{-1/2}. \quad (99)$$

If Compton processes were effective everywhere, this high value of the parameter ξ would imply that the plasma is Compton-heated to keV-temperatures out to very large distances of order 10^{12} cm. At large distances, however, the Compton heating time becomes longer than the characteristic time of gas accretion:

$$\frac{t_C}{t_{accr}} = \frac{t_C f(u) u_{ff}}{R} \approx 20 f(u)\dot{M}_{16}^{-1}R_{10}^{1/2}, \quad (100)$$

which indicates that Compton heating in a falling matter is ineffective. Consequently, the gas temperature is determined by photoionization heating only, and the gas can only be heated up to $T_{max}\approx5\times10^5$ K [66], which is substantially lower than $T_X\sim3$ keV.

The effective gravitational capture radius corresponding to the sound velocity of the gas in the photoionization-heated zone is expressed as

$$R_B^* = \frac{2GM}{c_s^2} = \frac{2GM}{\gamma\mathcal{R}T_{max}/\mu_m} \approx 3.5\times10^{12}\left(\frac{T_{max}}{5\times10^5\text{ K}}\right)^{-1}\text{ [cm]}. \quad (101)$$

Everywhere up to the bow shock, photoionization maintains the temperature at a value of $\simeq T_{max}$. The sound velocity corresponding to T_{max} reaches approximately 80 km s^{-1}. If the stellar wind velocity exceeds 80 km s^{-1}, a standard bow shock is formed at the Bondi radius with a post-shock temperature given by formula (94). If the stellar wind velocity is lower than this value, the shock disappears and quasispherical accretion occurs from R_B^*.

The photoionization heating time at the effective Bondi radius of 3×10^{12} cm is given by

$$t_{pi} \approx \frac{(3/2)kT_{max}/\mu_m}{(h\nu_{eff}-\zeta_{eff})n_\gamma\sigma_{eff}c} \approx 2\times10^4\dot{M}_{16}^{-1}\text{ [s]}. \quad (102)$$

Here, $h\nu_{eff}\sim10$ keV is the characteristic photon energy, ζ_{eff} is the effective photoionization potential, $\sigma_{eff}\sim10^{-24}$ cm^2 is the typical photoionization cross section, and $n_\gamma = L/(4\pi R^2 h\nu_{eff}c)$ is the photon number density. The photoionization-to-accretion time ratio at the effective Bondi radius is then equal to

$$\frac{t_{pi}}{t_{accr}} \approx 0.07 f(u)\dot{M}_{16}^{-1}. \quad (103)$$

At stellar wind velocities $v_w > 80$ km s^{-1}, the bow shock stands at the classical Bondi radius R_B inside the effective Bondi radius R_B^* determined by formula (101). The radiative

cooling time of the shocked plasma at R_B expressed through the wind velocity v_w equals

$$t_{cool} \approx 4.7 \times 10^4 \dot{M}_{16}^{-1} v_7^{0.2} \text{ [s]} . \quad (104)$$

The photoionization heating time in the post-shock region can also be expressed through the stellar wind velocity:

$$t_{pi} \approx 3.5 \times 10^4 \dot{M}_{16}^{-1} v_7^{-4} \text{ [s]} . \quad (105)$$

A comparison of these two characteristic timescales implies that radiative cooling becomes important at low wind velocities, where the source enters the regime of free-fall accretion with conservation of specific angular momentum of a falling matter.

Thus, the plasma behind the shock cools down at low wind velocities and starts to fall freely. As the cold plasma approaches the gravitating center, photoionization heating becomes important and rapidly heats up the plasma to $T_{max} \approx 5 \times 10^5$ K. Should this occur at a radius where $T_{max} < GM/(\mathcal{R}R)$, the plasma with a constant temperature T_{max} will continue its free fall down to the magnetosphere, with the subsequent formation of a shock above the magnetosphere. However, if $T_{max} > GM/(\mathcal{R}R)$, settling accretion will work even at low wind velocities.

For high stellar wind velocities, $v_w \gtrsim 100 \text{ km s}^{-1}$, the post-shock temperature is higher than T_{max}, photoionization heating is unimportant, and the settling accretion regime in the shell is established if the radiative cooling time is longer than the accretion time. From a comparison of these timescales, it is possible to find the critical accretion rate as a function of the wind velocity, the rate below which the settling accretion regime may come into play:

$$\dot{M}_{16}^{\ddagger} \lesssim 0.12 v_7^{3.2} . \quad (106)$$

Here, we stress the difference between the critical accretion rates $\dot{M}^{\ddagger}$ and $\dot{M}^{\dagger}$, derived earlier. For $\dot{M} > \dot{M}^{\ddagger}$, the plasma rapidly cools behind the shock in the gravitational capture region and free-fall accretion begins (unless photoionization heats the plasma to above the adiabatic value at some radius), while for $\dot{M} > \dot{M}^{\dagger} \simeq 4 \times 10^{16} \text{ g s}^{-1}$, determined by formula (33), a supersonic free-fall gap appears immediately above the neutron star magnetosphere.

6.2 Possibility of the propeller regime

The very slow rotation of the neutron stars in X-ray pulsars considered here (GX 1+4, GX 301-2, Vela X-1, SXP 1062, and 4U 2204+56) with $\omega^*(R_A) < \omega_K(R_A)$ (see Table 1) makes it hard for these sources to enter the propeller regime, where matter is ejected with parabolic velocities from the magnetosphere, and the neutron star spins down.

Let us therefore start by estimating the important ratio of viscous stresses ($\sim B_t B_p$) to the gas pressure ($\sim B_p^2$) at the magnetospheric boundary. This ratio is proportional to B_t/B_p [see formula (72)] and is always much smaller than 1 (see Table 1), i.e., only large-scale convective motions with the characteristic hierarchy of eddy scales by radius can be established in the shell. When $\omega^* > \omega_K(R_A)$, a centrifugal barrier is formed and accretion stops (the propeller regime). In this case, the maximum possible braking torque applied to the neutron star is of order $-K_2\mu^2/R_A^3$ due to the strong coupling between the plasma and the magnetic field. Notice that the interaction of the plasma with the magnetic field in the propeller regime is effected by strong coupling, i.e., the toroidal magnetic field component B_t is comparable to the poloidal component B_p.

It cannot be excluded that a hot iso-angular-momentum envelope retains in this case as well, which would then remove angular momentum from the rotating magnetosphere. If the characteristic cooling time of the gas in the envelope is short in comparison to the falling time of matter, the shell disappears, and one can expect the formation of a thin Keplerian 'storage' disc around the neutron star magnetosphere [68]. There is no accretion of matter through such a disc, and the latter only serves to remove angular momentum from the magnetosphere.

6.3 Hot shell effects in the X-ray spectrum and a real-time power spectrum

The spectra of X-ray pulsars are dominated by emission generated in the accretion columns near the NS surface. The hot optically thin shell produces its own thermal emission, but even if all gravitational energy of the falling matter were released in the shell, the ratio of the X-ray luminosity from the shell to that of the accretion column would be about that of the neutron star radius to the magnetosphere radius, i.e., one percent or less. In reality, the luminosity from the shell is much smaller. The shell should also scatter X-ray radiation from the accretion column, but for this effect to be substantial, the Comptonization parameter y must be around one. The Thomson depth in the shell is, however, very small. Indeed, from the mass continuity equation and formulas (30) for the Alfvén radius and (32) for the factor $f(u)$, we get

$$\tau_T = \int_{R_A}^{R_B} n_e(R) \sigma_T \, dR \approx 3.2 \times 10^{-3} \dot{M}_{16}^{8/11} \mu_{30}^{-2/11} .$$

Therefore, for the characteristic temperatures near the magnetosphere [see formula (4)], the parameter y is as follows:

$$y = \frac{4kT}{m_e c^2} \tau_T \approx 2.4 \times 10^{-3} .$$

This means that the X-ray spectrum formed in the region of energy conversion close to the surface of the neutron star is not expected to be significantly altered by scattering on electrons in the hot shell.

Large-scale convective motions in the shell introduce an intrinsic timescale on the order of the free-fall time, which could give rise to some features [e.g., quasiperiodic oscillations (QPOs)] in the power spectrum of variability. QPOs were reported in several X-ray pulsars (see paper [69] and references cited therein). However, the expected frequencies of any QPOs arising in our model would be on the order of 1 mHz — much lower than those reported.

A stronger effect could be the appearance of dynamical instability in the shell due to enhanced Compton cooling and, hence, an increased mass accretion rate through the shell. This might lead to a complete collapse of the shell, triggering an X-ray outburst with a duration similar to the free-fall timescale in the shell ($\sim$ 1000 s). Such a transient behavior is observed in the supergiant fast X-ray transients (SFXTs); see also paper [70]. The possible development of such a scenario depends on the specific parameters of the shell and needs to be further investigated.

6.4 Can accretion (prograde or retrograde) discs be present in these pulsars?

Our analysis of the sample of pulsars in Section 5 suggested that in a convective shell above the magnetosphere an iso-angular-momentum distribution is the most plausible. Therefore, we shall below consider only this case, i.e., the rotation law $\omega \sim R^{-2}$. As follows from equation (60), the equilibrium angular frequency of the neutron star at $\dot{\omega}^* = 0$ is

$$\omega_{\rm eq}^* = \omega_{\rm B} \frac{1}{1 - z/Z} \left(\frac{R_{\rm B}}{R_{\rm A}}\right)^2 . \tag{107}$$

We stress that such an equilibrium in our model is only possible when a convective shell is present. At high accretion rates, $\dot{M} > \dot{M}^{\dagger} \simeq 4 \times 10^{16}$ g s^{-1}, accretion proceeds in the free-fall regime (with no shell present).

The equilibrium period for an X-ray pulsar in the quasi-spherical settling accretion regime can be derived from formula (70):

$$P_{\rm eq} \simeq 1300\, \mu_{30}^{12/11} \left(\frac{P_{\rm b}}{10 \text{ days}}\right) \dot{M}_{16}^{-4/11} v_8^4 \text{ [s]} .$$

For standard disc accretion, the equilibrium period is given by

$$P_{\rm eq,\,d} \approx 7\, \mu_{30}^{6/7} \dot{M}_{16}^{-3/7} \text{ [s]} , \tag{108}$$

and the longer periods observed in some X-ray pulsars can, thus, if a disc is present, be explained only assuming a very high magnetic field of the neutron star. Retrograde accretion discs are also discussed in the literature (see, e.g., paper [30] and references cited therein). Torque reversals produced by temporary forming retrograde discs during accretion from a stellar wind can, in principle, lead to very long periods for X-ray pulsars, even with standard magnetic fields. Such retrograde discs could be formed as a result of presenting inhomogeneities in the captured stellar wind [8, 9]. The scenario could, theoretically, work for pulsars at a high accretion rate, too high for a hot envelop to form. In the case of GX 1 + 4, however, it is highly unlikely that a stable retrograde disk would be observed on a timescale much longer than the orbital period of a binary (see a more detailed discussion of this issue in Ref. [32]). For both GX 301-2 and Vela X-1 pulsars, the observed positive torque–luminosity correlation (see Figs 3 and 4) also rules out a retrograde disc in any of these systems.

To conclude this discussion section, we should mention that, in reality, all pulsars (including those considered above) demonstrate a complex quasistationary behavior with dips, outbursts, etc. These considerations are beyond the scope of this paper and definitely deserve further observational and theoretical studies.

7. Conclusions

In recent paper [14] we constructed a theoretical model for quasispherical subsonic accretion onto slowly rotating magnetized neutron stars. In this model, the accreting matter is gravitationally captured from the stellar wind of the optical companion and subsonically settles down onto the rotating magnetosphere, forming an extended quasistatic shell. This shell mediates the angular momentum removal from the rotating neutron star magnetosphere by large-scale convective motions. Depending on the angular velocity of the rotating matter close to the magnetospheric boundary, this type of accretion can cause the neutron star to either spin up or spin down.

A detailed analysis and comparison with observations of the two X-ray GX 301-2 and Vela X-1 pulsars, both demonstrating positive torque–luminosity correlations near the equilibrium neutron star spin period, give evidence that the convective motions are most likely strongly anisotropic, and the rotational velocities in the shell, $\omega \sim R^{-2}$, have a near iso-angular-momentum distribution. We notice that a statistical analysis of long-period X-ray pulsars with Be-components in SMC in paper [71] also favored the rotation law following $\omega \sim R^{-2}$. The accretion rate through the shell is determined by the ability of the plasma to enter inside the magnetosphere. The settling regime of accretion, which allows angular momentum removal from the neutron star magnetosphere, can be realized for moderate accretion rates: $\dot{M} < \dot{M}^{\dagger} \simeq 4 \times 10^{16}$ g s^{-1} (X-ray luminosity $L_{\rm X} < L_{\rm X}^{\dagger} \simeq 4 \times 10^{36}$ erg s^{-1}). At higher accretion rates, a free-fall gap above the neutron star magnetosphere appears due to rapid Compton cooling, and accretion becomes highly nonstationary.

From observations of the spin-up/spin-down rates (the angular rotation frequency derivative $\dot{\omega}^*$ or $\partial\dot{\omega}^*/\partial\dot{M}$ near the torque reversal) in slowly rotating equilibrium X-ray pulsars with known orbital periods, it is possible to determine the main dimensionless parameters of the model, as well as to estimate the magnetic field of the neutron star. Such analyses have revealed a good agreement between magnetic field estimates obtained using our model and those derived from cyclotron line measurements for the GX 301-2 and Vela X-1 pulsars.

Using measurements of the spin period and the orbital period, together with an estimate of the neutron star magnetic field, our model furthermore offers a possibility of estimating the stellar wind velocity of the companion, without the need for complex spectroscopic measurements. For nonequilibrium pulsars there is a maximum possible spin-down rate, depending on the spin period P^*, the orbital period $P_{\rm b}$, the neutron star magnetic field μ, and the wind velocity $v_{\rm w}$. For such pulsars, it is possible to estimate a lower limit on the neutron star magnetic field using the observed spin-down rate and X-ray luminosity. For the pulsars GX 1 + 4, SXP 1062, and 4U 2206 + 54 investigated here, our estimates are all in agreement with standard field values and observed cyclotron line measurements.

In our model for quasispherical subsonic accretion, long-term spin-up/spin-down episodes, as observed in some X-ray pulsars, can be quantitatively explained by a change in the mean mass accretion rate onto the neutron star (and the corresponding mean X-ray luminosity). Clearly, these changes are related to the stellar wind properties of the optical companion in these binaries.

The model also predicts the specific behavior of the variations in $\delta\dot{\omega}^*$, observed on top of a steady spin-up or spin-down, as a function of mass accretion rate fluctuations $\delta\dot{M}$. There is a critical accretion rate $\dot{M}_{\rm cr}$, below which an anticorrelation between $\delta\dot{\omega}^*$ and $\delta\dot{M}$ should occur (the case of the GX 1 + 4 pulsar at the steady spin-down state currently observed), and above which $\delta\dot{\omega}^*$ should correlate with $\delta\dot{M}$ fluctuations (the case of Vela X-1, GX 301-2, and GX 1 + 4 pulsars in the steady spin-up state). The model explains quantitatively the relative amplitude and the sign of the observed frequency fluctuations in the GX 1 + 4 pulsar.

8. Appendices

A. Structure of a quasispherical rotating shell with accretion

A.1 Basic equations

Let us first write down the Navier–Stokes equations in spherical coordinates R, θ, ϕ. Due to the huge Reynolds numbers in the shell ($\sim 10^{15}-10^{16}$ for a typical accretion rate of 10^{17} g s^{-1} and magnetospheric radius $\sim 10^8$ cm) there must be strong turbulence. In this case, the Navier–Stokes equations are usually called Reynolds equations. Generally, the turbulent viscosity may depend on the coordinates, so the hydrodynamical equations take the form:

(1) mass continuity equation

$$\frac{\partial\rho}{\partial t}+\frac{1}{R^2}\frac{\partial}{\partial R}(R^2\rho u_{\rm r})+\frac{1}{R\sin\theta}\frac{\partial}{\partial\theta}(\sin\theta\,\rho u_\theta)+\frac{1}{R\sin\theta}\frac{\partial\rho u_\phi}{\partial\phi}=0\,; \tag{A.1}$$

(2) R-component of the momentum equation

$$\frac{\partial u_{\rm r}}{\partial t}+u_{\rm r}\frac{\partial u_{\rm r}}{\partial R}+\frac{u_\theta}{R}\frac{\partial u_{\rm r}}{\partial\theta}+\frac{u_\phi}{R\sin\theta}\frac{\partial u_{\rm r}}{\partial\phi}-\frac{u_\phi^2+u_\theta^2}{R}=-\frac{GM}{R^2}+N_R\,; \tag{A.2}$$

(3) θ-component of the momentum equation

$$\frac{\partial u_\theta}{\partial t}+u_{\rm r}\frac{\partial u_\theta}{\partial R}+\frac{u_\theta}{R}\frac{\partial u_\theta}{\partial\theta}+\frac{u_\phi}{R\sin\theta}\frac{\partial u_\theta}{\partial\phi}+\frac{u_{\rm r}u_\theta-u_\phi^2\cot\theta}{R}=N_\theta\,; \tag{A.3}$$

(4) ϕ-component of the momentum equation

$$\frac{\partial u_\phi}{\partial t}+u_{\rm r}\frac{\partial u_\phi}{\partial R}+\frac{u_\theta}{R}\frac{\partial u_\phi}{\partial\theta}+\frac{u_\phi}{R\sin\theta}\frac{\partial u_\phi}{\partial\phi}+\frac{u_{\rm r}u_\phi+u_\phi u_\theta\cot\theta}{R}=N_\phi\,. \tag{A.4}$$

Here, the force components (including viscous force and gas pressure gradients) read as follows:

$$\rho N_R=\frac{1}{R^2}\frac{\partial}{\partial R}(R^2W_{RR})+\frac{1}{\sin\theta\,R}\frac{\partial}{\partial\theta}(W_{R\theta}\sin\theta)+\frac{1}{\sin\theta\,R}\frac{\partial}{\partial\phi}\,W_{R\phi}-\frac{W_{\theta\theta}}{R}-\frac{W_{\phi\phi}}{R}\,, \tag{A.5}$$

$$\rho N_\theta=\frac{1}{R^2}\frac{\partial}{\partial R}(R^2W_{\theta R})+\frac{1}{\sin\theta\,R}\frac{\partial}{\partial\theta}(W_{\theta\theta}\sin\theta)+\frac{1}{\sin\theta\,R}\frac{\partial}{\partial\phi}\,W_{\theta\phi}-\cot\theta\,\frac{W_{\theta\theta}}{R}\,, \tag{A.6}$$

$$\rho N_\phi=\frac{1}{R^3}\frac{\partial}{\partial R}(R^3W_{\phi R})+\frac{1}{\sin\theta\,R}\frac{\partial}{\partial\theta}(W_{\phi\theta}\sin\theta)+\frac{1}{\sin\theta\,R}\frac{\partial}{\partial\phi}\,W_{\phi\phi}\,. \tag{A.7}$$

The components of the stress tensor include a contribution from both the gas pressure $P_{\rm g}$ (assumed to be isotropic) and the turbulent pressure $P^{\rm t}$ (generally anisotropic). In defining them, we shall follow the classical treatment by Landau and Lifshitz [72], but with the inclusion of anisotropic turbulent pressure:

$$W_{RR}=-P_{\rm g}-P^{\rm t}_{RR}+2\rho v_{\rm t}\frac{\partial u_{\rm r}}{\partial R}-\frac{2}{3}\,\rho v_{\rm t}\,{\rm div}\,\mathbf{u}\,, \tag{A.8}$$

$$W_{\theta\theta}=-P_{\rm g}-P^{\rm t}_{\theta\theta}+2\rho v_{\rm t}\left(\frac{1}{R}\frac{\partial u_\theta}{\partial\theta}+\frac{u_{\rm r}}{R}\right)-\frac{2}{3}\,\rho v_{\rm t}\,{\rm div}\,\mathbf{u}\,, \tag{A.9}$$

$$W_{\phi\phi}=-P_{\rm g}-P^{\rm t}_{\phi\phi}+2\rho v_{\rm t}\left(\frac{1}{R\sin\theta}\frac{\partial u_\phi}{\partial\phi}+\frac{u_{\rm r}}{R}+\frac{u_\theta\cot\theta}{R}\right)-\frac{2}{3}\,\rho v_{\rm t}\,{\rm div}\,\mathbf{u}\,, \tag{A.10}$$

$$W_{R\theta}=\rho v_{\rm t}\left(\frac{1}{R}\frac{\partial u_{\rm r}}{\partial\theta}+\frac{\partial u_\theta}{\partial R}-\frac{u_\theta}{R}\right), \tag{A.11}$$

$$W_{\theta\phi}=\rho v_{\rm t}\left(\frac{1}{R\sin\theta}\frac{\partial u_\theta}{\partial\phi}+\frac{1}{R}\frac{\partial u_\phi}{\partial\theta}-\frac{u_\phi\cot\theta}{R}\right), \tag{A.12}$$

$$W_{R\phi}=\rho v_{\rm t}\left(\frac{1}{R\sin\theta}\frac{\partial u_{\rm r}}{\partial\phi}+\frac{\partial u_\phi}{\partial R}-\frac{u_\phi}{R}\right). \tag{A.13}$$

In our problem, the anisotropy of the turbulence is such that $P^{\rm t}_{RR}=P^{\rm t}_{\parallel}$, and $P^{\rm t}_{\theta\theta}=P^{\rm t}_{\phi\phi}=P^{\rm t}_{\perp}$. The turbulent pressure components can be expressed through turbulent Mach numbers and will be given in Appendix E.

In spherical coordinates, the divergence of vector $\mathbf{u}$ is written out as

$${\rm div}\,\mathbf{u}=\frac{1}{R^2}\frac{\partial}{\partial R}(R^2u_{\rm r})+\frac{1}{R\sin\theta}\frac{\partial}{\partial\theta}(\sin\theta\,u_\theta)+\frac{1}{R\sin\theta}\frac{\partial u_\phi}{\partial\phi}\,. \tag{A.14}$$

A.2 Symmetries of the problem

We shall consider axially symmetric ($\partial/\partial\phi=0$), stationary ($\partial/\partial t=0$), and purely radial ($u_\theta=0$) gas accretion. Under these conditions, from continuity equation (A.1) it follows that

$$\dot M=4\pi R^2\rho u_{\rm r}={\rm const}\,. \tag{A.15}$$

The constant here is determined by the conditions of plasma propagation through the magnetosphere.

Let us rewrite the Reynolds equations under the above assumptions. The R-component of momentum equation (A.2) becomes

$$\rho\left(u_{\rm r}\frac{\partial u_{\rm r}}{\partial R}-\frac{u_\phi^2}{R}\right)=-\rho\,\frac{GM}{R^2}+\frac{1}{R^2}\frac{\partial}{\partial R}(R^2W_{RR})+\frac{1}{\sin\theta\,R}\frac{\partial}{\partial\theta}(W_{R\theta}\sin\theta)-\frac{W_{\theta\theta}}{R}-\frac{W_{\phi\phi}}{R}\,; \tag{A.16}$$

the θ-component of the momentum equation becomes

$$-\rho\,\frac{u_\phi^2\cot\theta}{R}=\frac{1}{R^2}\frac{\partial}{\partial R}(R^2W_{\theta R})+\frac{1}{\sin\theta\,R}\frac{\partial}{\partial\theta}(W_{\theta\theta}\sin\theta)-\cot\theta\,\frac{W_{\theta\theta}}{R}\,, \tag{A.17}$$

and the ϕ-component of the momentum equation becomes

$$\rho\left(u_{\rm r}\frac{\partial u_\phi}{\partial R}+\frac{u_{\rm r}u_\phi}{R}\right)=\frac{1}{R^3}\frac{\partial}{\partial R}(R^3W_{\phi R})+\frac{1}{\sin\theta\,R}\frac{\partial}{\partial\theta}(W_{\phi\theta}\sin\theta)\,. \tag{A.18}$$

The components of the viscous stress tensor involving anisotropic turbulence take the form

$$W_{RR} = -P_{\rm g} - P_{\parallel}^{\rm t} - \frac{4}{3}\,\rho v_{\rm t}\left(\frac{u_{\rm r}}{R} - \frac{\partial u_{\rm r}}{\partial R}\right), \tag{A.19}$$

$$W_{\theta\theta} = -P_{\rm g} - P_{\perp}^{\rm t} + \frac{2}{3}\,\rho v_{\rm t}\left(\frac{u_{\rm r}}{R} - \frac{\partial u_{\rm r}}{\partial R}\right), \tag{A.20}$$

$$W_{\phi\phi} = -P_{\rm g} - P_{\perp}^{\rm t} + \frac{2}{3}\,\rho v_{\rm t}\left(\frac{u_{\rm r}}{R} - \frac{\partial u_{\rm r}}{\partial R}\right), \tag{A.21}$$

$$W_{R\theta} = \rho v_{\rm t}\,\frac{1}{R}\,\frac{\partial u_{\rm r}}{\partial \theta}\,, \tag{A.22}$$

$$W_{\theta\phi} = \rho v_{\rm t}\left(\frac{1}{R}\,\frac{\partial u_{\phi}}{\partial \theta} - \frac{u_{\phi}\cot\theta}{R}\right), \tag{A.23}$$

$$W_{R\phi} = \rho v_{\rm t}\left(\frac{\partial u_{\phi}}{\partial R} - \frac{u_{\phi}}{R}\right). \tag{A.24}$$

The main problem in describing gas-dynamic flows with developed turbulence consists in finding the kinematic viscosity parameter $v_{\rm t}$. As is well known, the viscosity parameter v in the case of laminar flows is dependent only on the properties of the medium (liquid or gas). When turbulence is present, however, this coefficient is also determined by the macroscopic properties of the flow itself. There are some empirical relations which, in principle, can be verified experimentally. Most often, the so-called turbulent mixing length $l_{\rm t}$ is introduced. Furthermore, Ludwig Prandtl in his work introduced for plane-parallel shear flows (along the x-axis, to be specific) the relationship between the turbulent mixing length $l_{\rm t}$, the velocity $u_{\rm t}$ of the turbulent flow, and the characteristic shear in the direction perpendicular to the averaged flow (z):

$$v_{\rm t} = C_0 l_{\rm t}\left|\frac{{\rm d}u}{{\rm d}z}\right|, \tag{A.25}$$

where $C_0 \sim 1$ is a universal dimensionless constant, the exact numerical value of which should be determined from a theory that currently does not exist. In this way, the dependence of the turbulent stresses on the shear value assumes the quadratic form:

$$W_{zx} = \rho C_0\left(\frac{{\rm d}u}{{\rm d}z}\right)^2,$$

and a nonlinearity emerges, which generally makes the problem a lot more difficult.

First, we consider the generalized Prandtl law for turbulent viscosity in the case of an axisymmetric flow. In the case of strong anisotropy, there is one more empirical law for describing the turbulent viscosity: the Wasiutyński law (see below), which is not reduced to the Prandtl law in the conditions of isotropic turbulence. This more general case for anisotropic turbulence will be discussed separately in Appendix C.

B. Structure of the shell in the case of turbulent viscosity according to the Prandtl law

B.1 Empirical Prandtl law for axisymmetric flows with turbulent viscosity

We consider an axisymmetric flow with a very large Reynolds number. By generalizing the Prandtl law for the turbulent velocities, inferred for plane-parallel flows, the turbulent velocity scales as $u_{\rm t} \sim l_{\rm t} R(\partial\omega/\partial R)$. From the similarity laws of gas dynamics, we assume $l_{\rm t} \sim R$, so that

$$u_{\rm t} = C_1 R^2\left|\frac{\partial\omega}{\partial R}\right|. \tag{B.1}$$

We notice that the turbulent velocity is determined in our case by convection, and thus $u_{\rm t} \lesssim 0.5 u_{\rm ff}$ (see Appendix D). This implies that the constant C_1 scales as

$$C_1 \sim \frac{u_{\rm t}}{\langle u_{\phi}\rangle} \tag{B.2}$$

and can be very large, since $\langle u_{\phi}\rangle \ll u_{\rm t}$. The turbulent viscosity coefficient reads then as

$$v_{\rm t} = \langle u_{\rm t} l_{\rm t}\rangle = C_2 C_1 R^3\left|\frac{\partial\omega}{\partial R}\right|. \tag{B.3}$$

Here, $C_2 \approx 1/3$ is a numerical factor originating from statistical averaging. Below, we shall combine C_1 and C_2 into the new coefficient $C = C_1 C_2$, which can be much larger than unity.

For such a viscosity prescription, the turbulent stresses $W_{R\phi}$ can be expressed as

$$W_{R\phi} = \rho v_{\rm t} R\,\frac{\partial\omega}{\partial R} = \rho C R^4\left(\frac{\partial\omega}{\partial R}\right)^2. \tag{B.4}$$

B.2 Angular momentum transport equation

A similar problem (that of a rotating sphere in a viscous fluid) was solved by Landau and Lifshitz [72]. They showed that the variables here become separated, and $u_{\phi}(R,\theta) = u_{\phi}(R)\sin\theta$. Notice that the angular velocity $\omega(R) = u_{\phi}(R)/R$ is independent of the polar angle θ. The setting of our problem is different from that of the sphere in a viscous fluid in several respects: (1) there is a force of gravity present; (2) the turbulent viscosity varies with R and can, in theory, depend on θ, and (3) there is radial motion of matter (accretion). These distinctions lead, as will be shown below, to the radial dependence of the rotational velocity: $u_{\phi}(R) \propto R^{-1/2}$. (We recall that $u_{\phi} \propto R^{-2}$ for a rotating sphere in a viscous fluid.)

Let us start with solving equation (A.18). First, we note that for $u_{\phi}(\theta) \sim \sin\theta$, according to formula (A.23), $W_{\theta\phi} = 0$. Further, making use of the continuity equation (E.8) and the definition of angular velocity, we rewrite equation (A.18) in the form of angular momentum transfer by viscous forces:

$$\sin\theta\,\frac{\dot{M}}{R}\,\frac{\partial}{\partial R}\,\omega R^2 = \frac{4\pi}{R}\,\frac{\partial}{\partial R}\,R^3 W_{R\phi}\,. \tag{B.5}$$

Recasting equation (A.24) in terms of the derivative of the angular velocity yields

$$W_{R\phi} = \rho v_{\rm t} R\,\frac{\partial\omega}{\partial R}\sin\theta\,. \tag{B.6}$$

Substituting this expression into equation (B.5) and integrating over R, we get

$$\dot{M}\omega R^2 = 4\pi\rho v_{\rm t} R^4\,\frac{\partial\omega}{\partial R} + D\,, \tag{B.7}$$

where D is an integration constant. This equation for angular momentum transport by turbulent viscosity is similar to that

for disc accretion [2], but different due to the spherical symmetry of our problem.

The left-hand side of equation (B.7) simply governs advection of specific angular momentum averaged over the sphere ($(1/2)\int_0^\pi \omega R^2 \sin^2\theta \sin\theta \,\mathrm{d}\theta = (1/3)\omega R^2$) by the average motion toward the gravitational center (accretion). The accretion rate $\dot{M}$ is then negative, as is $\partial\omega/\partial R$. The first term in the right-hand side of equation (B.7) describes the transport of angular momentum outwards by turbulent viscous forces.

The constant D is determined from the equation

$$D = \frac{K_1}{\zeta}\, K_2\, \frac{\mu^2}{R_\mathrm{A}^3}\, \frac{\omega_\mathrm{m} - \omega^*}{\omega_\mathrm{K}(R_\mathrm{A})} \tag{B.8}$$

[see formula (51) in Section 3.2]. We consider accretion onto a magnetized neutron star. When $D < 0$, the advection term in the left-hand side of equation (B.7) dominates over viscous angular momentum transfer outwards. Conversely, when $D > 0$, the viscous term in the right-hand side of equation (B.7) dominates. When $\dot{M} = 0$ (no plasma enters the magnetosphere), there is only angular momentum transport outwards by viscous forces.

Now let us rewrite equation (B.8) in the form

$$D = \frac{K_1}{\zeta}\, K_2\, \frac{\mu^2}{R_\mathrm{A}^6}\, R_\mathrm{A}^3\, \frac{\omega_\mathrm{m} - \omega^*}{\omega_\mathrm{K}(R_\mathrm{A})}\,, \tag{B.9}$$

and use the pressure balance condition

$$P(R_\mathrm{A}) = P_\mathrm{g}(R_\mathrm{A})(1 + \gamma m_\mathrm{t}^2) = \frac{B^2(R_\mathrm{A})}{8\pi} = \frac{K_2}{2\pi}\, \frac{\mu^2}{R_\mathrm{A}^6}\,. \tag{B.10}$$

Applying the mass continuity equation in the form

$$|\dot{M}| = 4\pi R^2 \rho f(u) \sqrt{\frac{GM}{R}}$$

and the expression for the gas pressure (8), we present the integration constant $D/|\dot{M}|$ in the form

$$\frac{D}{|\dot{M}|} = \frac{K_1}{\zeta}\, \frac{\gamma - 1}{\gamma}\, \psi(\gamma, m_\mathrm{t})\, \frac{(\omega_\mathrm{m} - \omega^*) R_\mathrm{A}^2}{2\sqrt{2}\, f(u)}\, (1 + \gamma m_\mathrm{t}^2)\,. \tag{B.11}$$

Let us consider the case where the neutron star rotates close to equilibrium with $\dot{\omega}^* = 0$. In this case, according to formula (58), one has

$$\omega_\mathrm{m} - \omega^* = -\frac{z}{Z}\, \omega^*\,, \tag{B.12}$$

and thus using the definition of Z (56), we obtain

$$\frac{D}{|\dot{M}|} = -z R_\mathrm{A}^2 \omega^*\,. \tag{B.13}$$

We would like to stress that the value of the constant D is fully determined in NS equilibrium rotating by the dimensionless specific angular momentum of matter at the Alfvén radius z.

B.3 Angular rotation law inside the shell

Let us now use equation (B.7) to find the rotation law $\omega(R)$. At large distances $R \gg R_\mathrm{A}$ (we would like to remind the reader that R_A is the bottom radius of the shell), the constant D is small compared to the other terms, so we can set $D \approx 0$. Thus, when obtaining the rotation law, we shall neglect this constant in the right-hand side of equation (B.7). Next, substituting expression (B.3) and the solution for the density (which, as we shall show below, remains the same as in the hydrostatic solution)

$$\rho(R) = \rho(R_\mathrm{A}) \left(\frac{R_\mathrm{A}}{R}\right)^{3/2} \tag{B.14}$$

into equation (B.7) yields

$$|\dot{M}|\omega R^2 = 4\pi\rho(R_\mathrm{A}) \left(\frac{R_\mathrm{A}}{R}\right)^{3/2} C R^7 \left(\frac{\partial\omega}{\partial R}\right)^2. \tag{B.15}$$

After integrating this equation, we find

$$2\omega^{1/2} = \pm\frac{4}{3}\, \frac{K^{1/2}}{R^{3/4}} + D_1\,, \tag{B.16}$$

where

$$K = \frac{|\dot{M}|}{4\pi\rho(R_\mathrm{A}) C R_\mathrm{A}^{3/2}}\,, \tag{B.17}$$

and D_1 is some integration constant. In equation (B.16), we make use only of the positive solution (the minus sign with constant $D_1 > 0$ would correspond to a solution with the angular velocity growing outwards, which is possible if the pulsar has a very long spin period, i.e., barely rotates at all). If $D_1 \neq 0$, for large $R \gg R_\mathrm{A}$ (in the zone close to the bow shock) the solid-body rotation law would lead to $\omega \to \mathrm{const} \approx \omega_\mathrm{B}$. (However, we remind the reader that our discussion is not applicable close to the bow shock region.) At small distances from the Alfvénic surface, the effect of the constant D_1 is small, and we shall neglect it in the calculations below. Then, we obtain

$$\omega(R) = \frac{4}{9}\, \frac{|\dot{M}|}{4\pi\rho(R_\mathrm{A}) C R_\mathrm{A}^3} \left(\frac{R_\mathrm{A}}{R}\right)^{3/2}, \tag{B.18}$$

i.e., the quasi-Keplerian law of rotation: $\omega(R) = \omega_\mathrm{m}(R_\mathrm{A}/R)^{3/2}$. The quantity ω_m in the solution given by equation (B.18) is determined after substituting $\dot{M}$ from the continuity equation at $R = R_\mathrm{A}$ into equation (B.18):

$$\omega_\mathrm{m} \equiv \tilde{\omega}\omega(R_\mathrm{A}) = \frac{4}{9}\, \tilde{\omega}\, \frac{|u_\mathrm{r}(R_\mathrm{A})|}{C R_\mathrm{A}}\,. \tag{B.19}$$

Here, we have introduced the correction factor $\tilde{\omega} > 1$ to account for the deviation of the exact solution from the Keplerian law in the vicinity of R_A.

Because radial velocity $u_\mathrm{r}(R_\mathrm{A})$ is smaller than the free-fall velocity, the above formula implies that $\omega_\mathrm{m} < \omega_\mathrm{K}(R_\mathrm{A})$, i.e. lower than the Keplerian angular frequency. For self-consistency, coefficient C in the Prandtl law may be determined, according to formula (B.19), from the ratio of the radial velocity u_r to the rotational velocity of matter u_ϕ:

$$C = \frac{4}{9}\, \tilde{\omega}\, \frac{|u_\mathrm{r}(R_\mathrm{A})|}{\omega_\mathrm{m} R_\mathrm{A}} = \frac{4}{9}\, \tilde{\omega}\, \frac{|u_\mathrm{r}(R_\mathrm{A})|}{u_\phi(R_\mathrm{A})}\,. \tag{B.20}$$

We note that this ratio is independent of the radius R and is actually constant across the shell. Indeed, the radial dependence of the velocity u_r follows from the continuity equation

with account for the density distribution (B.14):

$$u_{\rm r}(R) = u_{\rm r}(R_{\rm A})\left(\frac{R_{\rm A}}{R}\right)^{1/2}. \tag{B.21}$$

For a quasi-Keplerian law, $u_\phi(R) \sim 1/R^{1/2}$, so the ratio $u_{\rm r}/u_\phi$ remains constant.

Finally, the angular frequency $\omega_{\rm m}$ of the rotation of the shell near the magnetosphere is related to the angular frequency of the motion of matter near the bow shock as

$$\omega_{\rm m} = \tilde{\omega}\omega_{\rm B}\left(\frac{R_{\rm B}}{R_{\rm A}}\right)^{3/2}. \tag{B.22}$$

In reality, when approaching $R_{\rm A}$, the integration constant D (which we neglected at large distances $R \gg R_{\rm A}$) should be taken into account. The rotational law will thus somewhat differ from a quasi-Keplerian law close to the magnetosphere.

We stress the principal difference between this regime of accretion and disc accretion. For disc accretion, the radial velocity of motion of matter is much smaller than the turbulent velocity, and the tangential velocity is almost Keplerian and is much larger than the turbulent velocity. The radial velocity in the quasispherical subsonic accretion is not determined by the rate of the angular momentum removal. It is only determined by the 'permeability' of the neutron star magnetosphere to infalling matter. In our case, we assume that the radial velocity is on the order of the velocity of convective motions in the shell. The tangential velocity for the obtained quasi-Keplerian law is much smaller than the velocity of the convective motions. Note also that in the event of disc accretion the turbulence can be parametrized by only one dimensionless parameter, $\alpha \approx u_{\rm t}^2/u_{\rm s}^2$, with $0 < \alpha < 1$ [2]. The matter in an accretion disc rotates differentially with a supersonic (almost Keplerian) velocity, while in our case the shell rotates differentially with a velocity clearly lower than the subsonic velocity at any radius, and the turbulence in the shell is essentially subsonic. Also, our case with an extended shell is, of course, strongly different from the regime of freely falling matter with a standing shock above the magnetosphere [17].

B.4 The case without accretion

Now let us consider the case where the plasma cannot enter the magnetosphere and no accretion onto the neutron star occurs. This case is similar to the subsonic propeller regime considered by Davies and Pringle [11]. Equation (B.7) then takes the form

$$0 = 4\pi\rho v_{\rm t} R^4 \frac{\partial\omega}{\partial R} + D. \tag{B.23}$$

(Remember that the constant D is determined by the spin-down rate of the neutron star: $D = I\dot{\omega}^* < 0$.) Solving this equation as before, we arrive at the rotation law without accretion:

$$\omega(R) = \omega_{\rm m}\left(\frac{R_{\rm A}}{R}\right)^{7/4}, \tag{B.24}$$

where

$$\omega_{\rm m} = \frac{I|\dot{\omega}^*|}{7\pi\rho(R_{\rm A})v_{\rm t}(R_{\rm A})R_{\rm A}^3}. \tag{B.25}$$

From expression (B.3) one finds

$$v_{\rm t}(R_{\rm A}) = \frac{7}{4} C\omega_{\rm m} R_{\rm A}^2, \tag{B.26}$$

and, thus, for $\omega_{\rm m}$ we obtain

$$\omega_{\rm m} = \frac{2}{7}\left(\frac{I|\dot{\omega}^*|}{\pi C\rho(R_{\rm A})R_{\rm A}^5}\right)^{1/2}. \tag{B.27}$$

Alternatively, $\omega_{\rm m}$ is also related to the bow-shock region parameters as

$$\omega_{\rm m} = \omega_{\rm B}\left(\frac{R_{\rm B}}{R_{\rm A}}\right)^{7/4}. \tag{B.28}$$

The last relationship can, in principle, be used to further analyze this case, which we shall not do here.

C. Structure of the shell and angular rotation law for other turbulent viscosity prescriptions

C.1 Iso-angular-momentum rotation in the shell for isotropic viscosity

We would like to point out the possibility of having an iso-angular-momentum differential rotation in the shell, $\omega = \text{const}/R^2$, for the standard turbulent viscosity prescription in the form $\nu_{\rm t} \sim u_{\rm t} l_{\rm t}$ without using the Prandtl law. Indeed, using the scaling for turbulent pulsations in the hot quasispherical shell, viz. $l_{\rm t} \sim R$, $u_{\rm t} \sim u_{\rm s} \sim R^{-1/2}$, as well as the density dependence $\rho \sim R^{-3/2}$ (5), from equation (B.7) it is easily seen that for $\dot{M} = \text{const}$ and $D = \text{const}$ the solution $\omega(R) \sim 1/R^2$ takes place. In the next section, we will show that the iso-angular-momentum rotation law can be realized in the shell for a more complicated form of the stress tensor components $W_{R\phi}$ in the case of anisotropic turbulence.

C.2 Angular rotation law for turbulent viscosity according to Wasiutyński

Prandtl's law for viscosity that was used above relates the scale and velocity of turbulent pulsations with the average angular velocity and is successfully applied when the turbulence is generated by the shear flow itself. In our problem, the turbulence is initiated by large-scale convective motions in the shell in the gravitational field. Due to radial convection, strong anisotropic turbulent motions may appear (the radial dispersion of chaotic motions could be much larger than the dispersion in the tangential direction), and Prandtl's law may thus be inapplicable. Anisotropic turbulence is much more complicated and remains poorly studied.

As a first step, we may adopt the empirical law for the component $W_{R\phi}$ of viscous stress tensor as suggested by Wasiutyński [73]:

$$\frac{W_{R\phi}}{\rho} = \left[\nu_{\rm t}\frac{{\rm d}\omega}{{\rm d}R} + (\nu_{\rm r} - \nu_{\rm t})\frac{{\rm d}(\omega R^2)}{{\rm d}R}\right]\sin\theta, \tag{C.1}$$

or

$$W_{R\phi} = \left[2\rho(-\nu_{\rm t} + \nu_{\rm r})\omega + \nu_{\rm r}\rho R\frac{{\rm d}\omega}{{\rm d}R}\right]\sin\theta, \tag{C.2}$$

where the radial and tangential kinematic viscosity coefficients are

$$\nu_{\rm r} = C_{\parallel}\langle|u_{\parallel}^{\rm t}|\rangle R,$$

$$\nu_{\rm t} = C_{\perp}\langle|u_{\perp}^{\rm t}|\rangle R,$$

respectively. The dimensionless constants $C_\parallel$ and $C_\perp$ are of the order of unity. In the isotropic case, one has $v_r = v_t$, $W_{R\phi} \sim \mathrm{d}\omega/\mathrm{d}R$, and in the strongly anisotropic case $v_r \gg v_t$, $W_{R\phi} \sim \mathrm{d}(\omega R^2)/\mathrm{d}R$. Using these definitions, let us substitute expression (C.2) into equation (B.5), and after integration over R rewrite the latter in the form

$$\omega R^2\left(1-\frac{2C_\perp\langle|u_\perp^t|\rangle}{|u_r|}\right)=C_\parallel\frac{\langle|u_\parallel^t|\rangle}{|u_r|}\frac{R\,\mathrm{d}(\omega R^2)}{\mathrm{d}R}-\frac{D}{|\dot M|}\,. \quad \text{(C.3)}$$

We notice that, due to self-similarity in the shell structure, $u_\parallel^t \sim u_\perp^t \sim u_r \sim R^{-1/2}$, and thus the ratios $\langle|u_\parallel^t|\rangle/u_r$ and $\langle|u_\perp^t|\rangle/u_r$ are constant. In this case, the obvious solution to the above equation reads as

$$\omega R^2+\frac{D}{|\dot M|}\frac{1}{1-2C_\perp\langle|u_\perp^t|\rangle/|u_r|} =\left(\omega_B R_B^2+\frac{D}{|\dot M|}\frac{1}{1-2C_\perp\langle|u_\perp^t|\rangle/|u_r|}\right) \times\left(\frac{R_B}{R}\right)^{|u_r|/(C_\parallel\langle|u_\parallel^t|\rangle)(1-2C_\perp\langle|u_\perp^t|\rangle/|u_r|)} \quad \text{(C.4)}$$

[here, the integration constant is defined in such a way that $\omega(R_B)=\omega_B$].

Now, let us analyze the equilibrium situation where $\dot\omega^* = 0$. In this case, as we remember, the following relations are valid:

$$\frac{D}{|\dot M|}=-z\omega^* R_A^2\,,\qquad \omega_m=\left(1-\frac{z}{Z}\right)\omega^*\,.$$

First, let us consider the case of strongly anisotropic, almost radial turbulence, where $\langle|u_\perp^t|\rangle = 0$. In this case, the specific angular momentum at the Alfvén radius takes the form

$$\omega_m R_A^2\left\{1+\frac{z}{1-z/Z}\left[\left(\frac{R_B}{R_A}\right)^{|u_r|/(C_\parallel\langle|u_\parallel^t|\rangle)}-1\right]\right\} =\omega_B R_B^2\left(\frac{R_B}{R_A}\right)^{|u_r|/(C_\parallel\langle|u_\parallel^t|\rangle)}\,. \quad \text{(C.5)}$$

From this it is seen that in the case of very weak accretion (or, in the limit when there is no accretion through the magnetosphere at all), the inequality $|u_r| \ll C_\parallel\langle|u_\parallel^t|\rangle$ is satisfied, and an almost iso-angular-momentum distribution of rotational velocities in the shell is formed.

The next case relates to situation where the amount of anisotropy is such that $C_\perp\langle|u_\perp^t|\rangle/|u_r| = 1/2$. Then, we have a strict iso-angular-momentum distribution in the shell: $\omega_m R_A^2 = \omega_B R_B^2$.

If the turbulence is fully isotropic, then

$$C_\perp\langle|u_\perp^t|\rangle = C_\parallel\langle|u_\parallel^t|\rangle = \tilde C\langle|u^t|\rangle\,.$$

Denoting $\epsilon = |u_r|/(\tilde C\langle|u^t|\rangle)$, we obtain

$$\omega_m R_A^2\left\{1+\frac{z}{1-z/Z}\frac{1}{2/\epsilon-1}\left[1-\left(\frac{R_A}{R_B}\right)^{2-\epsilon}\right]\right\} =\omega_B R_B^2\left(\frac{R_A}{R_B}\right)^{2-\epsilon}\,. \quad \text{(C.6)}$$

Notice that if $\epsilon \to 0$ (and there is no accretion through the magnetosphere), then $\omega_m \to \omega_B$, and we are dealing with solid-body rotation without accretion (cf. the first case above!). For $\epsilon = 3/2$, an almost quasi-Keplerian angular rotation distribution may be established. We remind the reader that a similar quasi-Keplerian distribution was obtained above in Appendix B with making use of the Prandtl law for isotropic turbulent viscosity. In that case, this was the only solution. Here, in contrast, the quasi-Keplerian law governs only one particular case of the general solution obtained using Wasiutyński's prescription for anisotropic turbulent viscosity.

As we have shown in Section 5, a quasi-Keplerian rotation law is not favored by observations. We therefore conclude that the most likely velocity distribution in the shell is the near iso-angular-momentum one, with anisotropic turbulence initiated by convection. Notice that for thin accretion discs, where the vertical height limits the scale of the turbulence, the Prandtl law for viscosity works very well [2].

D. Corrections to the radial temperature gradient

Here, we shall estimate how the radial temperature gradient differs from the adiabatic law due to convective motions in the shell. Multiplying equation (55) by $(1/2)(\omega_m - \omega^*)$, we obtain the convective heating rate caused by interaction of the shell with the magnetosphere:

$$L_c=\frac{1}{2}\,Z\dot M R_A^2(\omega_m-\omega^*)^2\,. \quad \text{(D.1)}$$

Multiplying the same equation (55) by ω^* yields the rate of change of the mechanical energy of the neutron star:

$$L_k = Z\dot M R_A^2\omega^*(\omega_m-\omega^*)\,. \quad \text{(D.2)}$$

The total energy balance is then written down as

$$L_t = L_c + L_k = \frac{1}{2}\,Z\dot M R_A^2(\omega_m^2-\omega^{*2})\,. \quad \text{(D.3)}$$

Notice that the obtained formula for L_c is similar to the equation describing energy release in the boundary layer of an accretion disc [74].

The convective energy flux is given by

$$q_c=\frac{L_c}{4\pi R^2}=\frac{Z\dot M R_A^2(\omega_m-\omega^*)^2}{8\pi R^2}\,. \quad \text{(D.4)}$$

On the other hand, the convective energy flux can be related to the entropy gradient as [75]

$$q_c=-\rho v_c T\frac{\mathrm{d}S}{\mathrm{d}R}\,, \quad \text{(D.5)}$$

where S is the specific entropy (per gram). Here, v_c is the radial turbulent heat conductivity:

$$v_c=\langle u_c l_c\rangle = C_h u_c R\,, \quad \text{(D.6)}$$

where the characteristic scale of convection $l_c \sim R$, the velocity of convective motions $u_c \sim c_s \sim R^{-1/2}$, and C_h is a numerical coefficient on the order of unity. Thus, one finds

$$v_c = v_c(R_A)\left(\frac{R}{R_A}\right)^{1/2}\,. \quad \text{(D.7)}$$

Next, we make use of the thermodynamic identity for the specific enthalpy H:

$$\frac{\mathrm{d}H}{\mathrm{d}R}=\frac{1}{\rho}\frac{\mathrm{d}P_\mathrm{g}}{\mathrm{d}R}+T\frac{\mathrm{d}S}{\mathrm{d}R}\,. \tag{D.8}$$

We remind the reader that the enthalpy can be written out as

$$\mathrm{d}H=c_p\,\mathrm{d}T\,,$$

where

$$c_p=T\left(\frac{\partial S}{\partial T}\right)_p=\frac{\gamma}{\gamma-1}\frac{\mathcal{R}}{\mu_\mathrm{m}}$$

is the specific heat capacity at constant pressure. Expressing $T(\mathrm{d}S/\mathrm{d}R)$ from equation (D.5) and making use of hydrostatic equilibrium equation (4) written as

$$\frac{\mathrm{d}P_\mathrm{g}/\rho}{\mathrm{d}R}=-\frac{\mathcal{R}}{\mu_\mathrm{m}c_p}\frac{GM}{R^2}\,\psi(\gamma,m_\mathrm{t})\,,$$

thermodynamic identity (D.8) can be rewritten in the form

$$\frac{\mathrm{d}T}{\mathrm{d}R}=-\frac{1}{c_p}\left[\frac{GM}{R^2}\,\psi(\gamma,m_\mathrm{t})-\frac{Zu_\mathrm{r}(R_\mathrm{A})}{2v_\mathrm{c}(R_\mathrm{A})}\frac{R_\mathrm{A}}{R}\,R_\mathrm{A}^2(\omega_\mathrm{m}-\omega^*)^2\right]. \tag{D.9}$$

By definition, the adiabatic temperature gradient is determined by the first term in the right-hand side of identity (D.9): $(\mathrm{d}T/\mathrm{d}R)_\mathrm{ad}=g/c_p$. Equation (D.9) can be integrated to find the actual dependence of the temperature on the radius in the convective shell:

$$T=\frac{1}{c_p}\left[\frac{GM}{R}\,\psi(\gamma,m_\mathrm{t})-\frac{Zu_\mathrm{r}(R_\mathrm{A})}{2v_\mathrm{c}(R_\mathrm{A})}\,R_\mathrm{A}^3(\omega_\mathrm{m}-\omega^*)^2\ln\frac{R}{R_\mathrm{A}}\right]. \tag{D.10}$$

Close to equilibrium ($I\dot{\omega}^*=0$), we make use of formula (B.12) and write out the dependence required:

$$T=\frac{1}{c_p}\left(\frac{GM}{R}\,\psi(\gamma,m_\mathrm{t})-\frac{u_\mathrm{r}(R_\mathrm{A})}{2C_\mathrm{h}u_\mathrm{c}(R_\mathrm{A})}\,\omega^{*2}R_\mathrm{A}^2\,\frac{z^2}{Z}\ln\frac{R}{R_\mathrm{A}}\right). \tag{D.11}$$

This solution implies that the temperature distribution for slowly rotating pulsars [i.e., in which $\omega_\mathrm{m}\ll\omega_\mathrm{K}(R_\mathrm{A})$] in the whole region between R_A and R_B is closely approximated by the adiabatic law with a temperature gradient close to the adiabatic one (4):

$$T\approx\frac{\gamma-1}{\gamma}\,\frac{GM}{\mathcal{R}R}\,\psi(\gamma,m_\mathrm{t})\,. \tag{D.12}$$

Here, we have only taken into account energy release due to the angular frequency difference near the magnetosphere. In reality, there may be additional sources of energy in the shell [the heat release during magnetic reconnection and turbulence (see Appendix E), etc.].

E. Dynamics of a stationary spherically symmetric ideal gas flow

In this appendix, we write down the gas-dynamic equations of a spherically symmetric ideal gas flow onto a Newtonian gravitating center. This problem was considered in 1952 in the classical paper by Bondi [18] for an adiabatic accretion flow. Adiabatic gas outflows (stellar winds) were studied later by Parker [76]. A thorough and comprehensible discussion of such flows can be found in the monograph by V S Beskin [77]. Here, we focus on the role of the cooling/heating processes near the Alvénic surface, and also take into account the effects of turbulence and/or convection (anisotropy in general). As discussed in the main text (see Section 4), the quasistatic shell at low X-ray luminosities is capable of removing angular momentum from the rotating magnetosphere via convective motions. As the accretion rate exceeds some critical value, strong Compton cooling causes a free-fall gap to appear above the magnetosphere, and angular momentum cannot be transferred from the magnetosphere to the shell any more.

Equation of motion (A.16) in the absence of viscosity reads as

$$u_\mathrm{r}\frac{\mathrm{d}u_\mathrm{r}}{\mathrm{d}R}=-\frac{1}{\rho}\frac{\mathrm{d}P_\mathrm{g}}{\mathrm{d}R}-\frac{1}{\rho}\frac{\mathrm{d}P_\parallel^\mathrm{t}}{\mathrm{d}R}-\frac{2(P_\parallel^\mathrm{t}-P_\perp^\mathrm{t})}{\rho R}-\frac{GM}{R^2}\,. \tag{E.1}$$

Here, $P_\mathrm{g}=\rho c_\mathrm{s}^2/\gamma$ is the gas pressure, and P^t is the pressure due to turbulent pulsations which in general are anisotropic:

$$P_\parallel^\mathrm{t}=\rho\langle u_\parallel^2\rangle=\rho m_\parallel^2c_\mathrm{s}^2=\gamma P_\mathrm{g}m_\parallel^2\,, \tag{E.2}$$

$$P_\perp^\mathrm{t}=2\rho\langle u_\perp^2\rangle=2\rho m_\perp^2c_\mathrm{s}^2=2\gamma P_\mathrm{g}m_\perp^2\,, \tag{E.3}$$

where $\langle u_\mathrm{t}^2\rangle=\langle u_\parallel^2\rangle+2\langle u_\perp^2\rangle$ is the turbulent velocity dispersion, and $m_\parallel^2$ and $m_\perp^2$ are the parallel and perpendicular turbulent Mach numbers squared).

From the first law of thermodynamics, we have

$$\frac{\mathrm{d}E}{\mathrm{d}R}=\frac{P_\mathrm{g}}{\rho}\frac{\mathrm{d}\rho}{\mathrm{d}R}+T\frac{\mathrm{d}S}{\mathrm{d}R}\,, \tag{E.4}$$

where the specific internal energy (per gram) is defined as

$$E=c_VT=\frac{c_\mathrm{s}^2}{\gamma(\gamma-1)}\,, \tag{E.5}$$

and the heat capacity is given by

$$c_V=\frac{\mathcal{R}}{\mu_\mathrm{m}}\frac{1}{\gamma-1}\,. \tag{E.6}$$

From the second law of thermodynamics, the specific entropy change can be written out through the rate of the specific heat change $\mathrm{d}Q/\mathrm{d}t$ [erg s^{-1} g^{-1}] as

$$T\frac{\mathrm{d}S}{\mathrm{d}R}=\frac{\mathrm{d}Q}{\mathrm{d}R}=\frac{\mathrm{d}Q/\mathrm{d}t}{u_\mathrm{r}}\,. \tag{E.7}$$

Using the mass continuity equation

$$\dot{M}=4\pi R^2\rho u_\mathrm{r}\,, \tag{E.8}$$

we arrive at

$$\frac{1}{\rho}\frac{\mathrm{d}\rho}{\mathrm{d}R}=-\frac{2}{R}-\frac{1}{2u_\mathrm{r}^2}\frac{\mathrm{d}u_\mathrm{r}^2}{\mathrm{d}R}\,. \tag{E.9}$$

Utilizing the relation $c_\mathrm{s}^2=\gamma\mathcal{R}T$, we finally obtain

$$\frac{1}{c_\mathrm{s}^2}\frac{\mathrm{d}c_\mathrm{s}^2}{\mathrm{d}R}=(\gamma-1)\left(-\frac{2}{R}-\frac{1}{2u_\mathrm{r}^2}\frac{\mathrm{d}u_\mathrm{r}^2}{\mathrm{d}R}\right)+\frac{\mathrm{d}Q/\mathrm{d}t}{u_\mathrm{r}c_VT}\,. \tag{E.10}$$

Notice that this equation can also be derived directly from the ideal gas equation of state written in the form

$$P_{\rm g} = K \exp\left(\frac{S}{c_V}\right)\rho^{\gamma}\,, \tag{E.11}$$

where K is some constant.

Making use of equation (E.10), the gas pressure gradient can be rewritten in the form

$$\frac{1}{P_{\rm g}}\,\frac{{\rm d}P_{\rm g}}{{\rm d}R} = \frac{c_{\rm s}^2}{c_V u_{\rm r}}\,\frac{{\rm d}Q/{\rm d}t}{T} + c_{\rm s}^2\left(-\frac{2}{R} - \frac{1}{2u_{\rm r}^2}\,\frac{{\rm d}u_{\rm r}^2}{{\rm d}R}\right). \tag{E.12}$$

Plugging (E.12) into the equation of motion finally yields

$$\frac{1}{2}\,\frac{1}{u_{\rm r}^2}\,\frac{{\rm d}u_{\rm r}^2}{{\rm d}R} = \left[c_{\rm s}^2(1+\gamma m_{\parallel}^2)\left(\frac{2}{R} - \frac{{\rm d}Q/{\rm d}t}{c_V u_{\rm r} T}\right) - 2c_{\rm s}^2\,\frac{m_{\parallel}^2 - m_{\perp}^2}{R} - \frac{GM}{R^2}\right]\left[u_{\rm r}^2 - c_{\rm s}^2(1+\gamma m_{\parallel}^2)\right]^{-1}. \tag{E.13}$$

Note also that in the strongly anisotropic case, where $m_{\parallel}^2 = m_{\rm t}^2 \gg m_{\perp}^2$, the role of turbulence enhances in comparison with the isotropic case, where $m_{\parallel}^2 = m_{\perp}^2 = (1/3)m_{\rm t}^2$.

We can also introduce the Mach number in the flow, $\mathcal{M} \equiv u_{\rm r}/c_{\rm s}$. Then, we derive from equations (E.10) and (E.13) the equation for the Mach number:

$$\frac{\mathcal{M}^2 - (1+\gamma m_{\parallel}^2)}{\mathcal{M}^2}\,\frac{{\rm d}\mathcal{M}^2}{{\rm d}R} = \frac{2\left[(\gamma-1)\mathcal{M}^2 - (\gamma+1)(m_{\parallel}^2 - m_{\perp}^2)\right]}{R} - \frac{\mathcal{M}^2 + \gamma(1+\gamma m_{\parallel}^2)}{c_V T}\,\frac{{\rm d}Q}{{\rm d}R} - \frac{(\gamma+1)GM}{R^2 c_{\rm s}^2}\,, \tag{E.14}$$

where we have substituted $u_{\rm r}({\rm d}Q/{\rm d}R)$ for ${\rm d}Q/{\rm d}t$. Equations (E.10), (E.13), and (E.14) can be employed in solving the dynamics of the accretion flow for pairs of independent variables $(u_{\rm r}, c_{\rm s})$, $(u_{\rm r}, \mathcal{M})$, or $(c_{\rm s}, \mathcal{M})$. Here, however, we shall only consider the behavior of the flux near the singular point. To this end, we can use equation (E.13).

Equation (E.13) has a singular saddle point where the denominator on its right-hand side vanishes:

$$u_{\rm r}^2 = c_{\rm s}^2(1+\gamma m_{\parallel}^2)\,. \tag{E.15}$$

The numerator on this side must do likewise, from which we find the quadratic equation for the flow velocity at the singular point:

$$u_{\rm r}^2\,\frac{2}{R}\,\frac{1+(\gamma-1)m_{\parallel}^2 + m_{\perp}^2}{1+\gamma m_{\parallel}^2} - u_{\rm r}\left(\frac{{\rm d}Q/{\rm d}t}{c_V T}\right) - \frac{GM}{R^2} = 0\,. \tag{E.16}$$

Remember that in the adiabatic case (${\rm d}Q/{\rm d}t = 0$) without turbulence at the saddle point we have simply

$$u_{\rm r}^2 = c_{\rm s}^2 = \frac{GM}{2R}\,. \tag{E.17}$$

It should be stressed that the presence of turbulence increases the velocity at the singular point. For example, for $\gamma = 5/3$ and strong anisotropic turbulence we find $u_{\rm r}^2 = c_{\rm s}^2(1 + (5/3)m_{\parallel}^2)$; the correction is smaller for isotropic turbulence: $u_{\rm r}^2 = c_{\rm s}^2(1 + (5/9)m_{\rm t}^2)$. The transition through the speed of sound (the sonic point where $u_{\rm r}^2 = c_{\rm s}^2$) lies above the saddle point due to turbulence, and there is no singularity at the sonic point.

Let us now determine the turbulence heating rate $({\rm d}Q/{\rm d}t)_{\rm t}^{+}$ in the quasistatic shell:

$$\left(\frac{{\rm d}Q}{{\rm d}t}\right)_{\rm t}^{+} = \frac{1}{2}\,\frac{\langle u_{\rm t}^2\rangle}{t_{\rm t}}\,, \tag{E.18}$$

where the characteristic time of the turbulent heating is expressed as

$$t_{\rm t} = \alpha_{\rm t}\,\frac{R}{u_{\rm t}} = \alpha_{\rm t}\,\frac{R}{m_{\rm t} c_{\rm s}}\,, \tag{E.19}$$

with $\alpha_{\rm t}$ being a dimensionless constant characterizing the turbulent dissipation energy rate, and the turbulent Mach number is $m_{\rm t}^2 \equiv m_{\parallel}^2 + 2m_{\perp}^2$. The turbulent heating rate can thus be written out as

$$\left(\frac{{\rm d}Q}{{\rm d}t}\right)_{\rm t}^{+} = \frac{c_{\rm s}^3}{2\alpha_{\rm t} R}\,m_{\rm t}^3\,. \tag{E.20}$$

In the case of Compton cooling, we have

$$\left(\frac{{\rm d}Q}{{\rm d}t}\right)_{\rm C}^{-} = -\frac{c_V(T - T_{\rm X})}{t_{\rm C}}\,, \tag{E.21}$$

where $t_{\rm C}$ is the characteristic Compton cooling time (16).

Equation (E.16) can now be presented in the form

$$u_{\rm r}^2\,\frac{2}{R}\,\frac{1+(\gamma-1)m_{\parallel}^2 + m_{\perp}^2}{1+\gamma m_{\parallel}^2} - u_{\rm r}^2\,\frac{c_{\rm s}}{u_{\rm r}}\,\frac{\gamma(\gamma-1)m_{\rm t}^3}{2\alpha_{\rm t} R} + \frac{u_{\rm r}(1 - T_{\rm X}/T)}{\gamma t_{\rm C}} - \frac{GM}{R^2} = 0\,. \tag{E.22}$$

As we study the accretion process, the sign of the velocity $u_{\rm r} = {\rm d}R/{\rm d}t$ is negative, so below we shall assume that $u_{\rm r} = -|u_{\rm r}|$. Then, for the absolute value of the flow velocity at the singular point, where the speed of sound is $c_{\rm s}/u_{\rm r} = -1/(1+\gamma m_{\parallel}^2)^{1/2}$, we have the quadratic equation:

$$u_{\rm r}^2\,\frac{2}{R}\,\frac{1+(\gamma-1)m_{\parallel}^2 + m_{\perp}^2}{1+\gamma m_{\parallel}^2} + u_{\rm r}^2\,\frac{1}{(1+\gamma m_{\parallel}^2)^{1/2}}\,\frac{\gamma(\gamma-1)m_{\rm t}^3}{2\alpha_{\rm t} R} - \frac{|u_{\rm r}|(1 - T_{\rm X}/T)}{\gamma t_{\rm C}} - \frac{GM}{R^2} = 0\,. \tag{E.23}$$

In this case, the solution to equation (E.16) reads as

$$|u_{\rm r}| = \frac{R(1 - T_{\rm X}/T)}{4\gamma t_{\rm C} A} + \sqrt{\frac{2GM}{R}}\left[\frac{1}{4A} + \frac{R}{2GM}\,\frac{R^2(1 - T_{\rm X}/T)^2}{16\gamma^2 t_{\rm C}^2 A^2}\right]^{1/2}, \tag{E.24}$$

where we have introduced the dimensionless factor

$$A = \frac{1+(\gamma-1)m_{\parallel}^2 + m_{\perp}^2}{1+\gamma m_{\parallel}^2} + \frac{\gamma(\gamma-1)(m_{\parallel}^2 + 2m_{\perp}^2)^{3/2}}{4\alpha_{\rm t}(1+\gamma m_{\parallel}^2)^{1/2}}\,. \tag{E.25}$$

In the case of isotropic turbulence, where $m_{\parallel} = m_{\perp} = 1/\sqrt{3}$, $m_{\rm t} = 1$, for $\gamma = 5/3$ the factor A takes the value ≈ 1.23, and in the case of strongly anisotropic turbulence, where $m_{\parallel} = 1$, $m_{\perp} = 0$, $m_{\rm t} = 1$, this factor is $A \approx 0.8$.

In units of the free-fall velocity, solution (E.24) assumes the form

$$f(u)=\frac{|u_{\rm r}|}{u_{\rm ff}}=\frac{1-T_{\rm X}/T}{4\gamma A}\,\frac{t_{\rm ff}}{t_{\rm C}}+\frac{1}{2}\left[\frac{1}{A}+\frac{(1-T_{\rm X}/T)^2}{4\gamma^2A^2}\left(\frac{t_{\rm ff}}{t_{\rm C}}\right)^2\right]^{1/2}. \tag{E.26}$$

With Compton cooling present, the temperature changes exponentially:

$$T=T_{\rm X}+(T_{\rm cr}-T_{\rm X})\exp\left(-\frac{t}{t_{\rm C}}\right) \tag{E.27}$$

(see Section 2.3). When cooling is slow, $t_{\rm ff}/t_{\rm C}\ll 1$, the critical point lies below the Alfvén surface, i.e., no transition through the critical point occurs in the flow before it meets the magnetosphere, and in this case we expect slow settling accretion. If this point lies above the Alfvén surface, the rate of the flow may become supersonic above the magnetosphere, and in circumstances where flow–magnetosphere interaction occurs one may expect the formation of a shock. Both turbulence and rapid cooling shift the location of the critical point upwards in the flow.

In the case of rapid cooling, one has $t_{\rm ff}/t_{\rm C}\gg 1$, $T\to T_{\rm X}$, so again $u_{\rm r}/u_{\rm ff}\approx 1/2$ [cf. formula (E.17) for an adiabatic flow], but the critical point now lies above the Alfvén surface, so a free-fall gap above the magnetosphere appears. The ratio $f(u)=|u_{\rm r}|/u_{\rm ff}$ reaches a maximum at $t_{\rm ff}/t_{\rm C}\approx 0.46$ (assuming a typical temperature ratio $T_{\rm cr}/T_{\rm X}=10$), and, depending on the value of $A=0.8-1.23$ (anisotropic or isotropic turbulence), it equals $f(u)=0.5-0.6$.

Acknowledgments

The authors would like to thank V A Doroshenko (IAAT) for courtesy providing the torque-luminosity plots for GX 301-2 and Vela X-1, and V S Beskin and V F Suleimanov for discussions. NISh thanks the Max Planck Institute for Astrophysics (Garching) for the hospitality. The work by NISh, KAP, and AYuK is supported by RFBR grants 09-02-00032, 12-02-00186, and 10-02-00599. LH is supported by a grant from the Wenner-Gren Foundation (Sweden).

References

1. Bildsten L et al. *Astrophys. J. Suppl.* **113** 367 (1997)
2. Shakura N I, Sunyaev R A *Astron. Astrophys.* **24** 337 (1973)
3. Pringle J E, Rees M J *Astron. Astrophys.* **21** 1 (1972)
4. Ghosh P, Lamb F K *Astrophys. J.* **234** 296 (1979)
5. Lovelace R V E, Romanova M M, Bisnovatyi-Kogan G S *Mon. Not. R. Astron. Soc.* **275** 244 (1995)
6. Kluźniak W, Rappaport S *Astrophys. J.* **671** 1990 (2007)
7. Fryxell B A, Taam R E *Astrophys. J.* **335** 862 (1988)
8. Ruffert M *Astron. Astrophys.* **317** 793 (1997)
9. Ruffert M *Astron. Astrophys.* **346** 861 (1999)
10. Burnard D J, Arons J, Lea S M *Astrophys. J.* **266** 175 (1983)
11. Davies R E, Pringle J E *Mon. Not. R. Astron. Soc.* **196** 209 (1981)
12. Illarionov A F, Kompaneets D A *Mon. Not. R. Astron. Soc.* **247** 219 (1990)
13. Bisnovatyi-Kogan G S *Astron. Astrophys.* **245** 528 (1991)
14. Shakura N, Postnov K, Kochetkova A, Hjalmarsdotter L *Mon. Not. R. Astron. Soc.* **420** 216 (2012)
15. Illarionov A F, Sunyaev R A *Astron. Astrophys.* **39** 185 (1975)
16. Elsner R F, Lamb F K *Astrophys. J.* **215** 897 (1977)
17. Arons J, Lea S M *Astrophys. J.* **207** 914 (1976)
18. Bondi H *Mon. Not. R. Astron. Soc.* **112** 195 (1952)
19. Arons J, Lea S M *Astrophys. J.* **210** 792 (1976)
20. Kompaneets A S *Sov. Phys. JETP* **4** 730 (1957) [*Zh. Eksp. Teor. Fiz.* **31** 876 (1956)]
21. Weymann R *Phys. Fluids* **8** 2112 (1965)
22. Shakura N, Postnov K, Hjalmarsdotter L *Mon. Not. R. Astron. Soc.* **428** 670 (2013)
23. Doroshenko V, Santangelo A, Suleimanov V *Astron. Astrophys.* **529** 52 (2011)
24. Finger M et al., http://gammaray.nsstc.nasa.gov/gbm/science/pulsars/lightcurves/gx1p4.html
25. Ikhsanov N R, Beskrovnaya N G *Astron. Rep.* **56** 589 (2012) [*Astron. Zh.* **89** 652 (2012)]
26. Lipunov V M *Astrophysics of Neutron Stars* (Berlin: Springer-Verlag, 1992) [Translated from Russian: *Astrofizika Neitronnykh Zvezd* (Moscow: Nauka, 1987)]
27. Chakrabarty D et al. *Astrophys. J. Lett.* **481** L101 (1997)
28. Sunyaev R A, in *Physics and Astrophysics of Neutron Stars and Black Holes* (Proc. of the Intern. School of Physics 'Enrico Fermi', Course 65, Eds R Giacconi, R Ruffini) (Amsterdam: North-Holland Publ. Co., 1978) p. 697
29. Ho C et al. *Mon. Not. R. Astron. Soc.* **238** 1447 (1989)
30. Nelson R W et al. *Astrophys. J.* **488** L117 (1997)
31. Hunt R *Mon. Not. R. Astron. Soc.* **154** 141 (1971)
32. González-Galán A et al. *Astron. Astrophys.* **537** A66 (2012)
33. Koh D T et al. *Astrophys. J.* **479** 933 (1997)
34. White N E et al. *Astrophys. J.* **209** L119 (1976)
35. Kaper L, van der Meer A, Najarro F *Astron. Astrophys.* **457** 595 (2006)
36. de Kool M, Anzer U *Mon. Not. R. Astron. Soc.* **262** 726 (1993)
37. Nagase F *Publ. Astron. Soc. Jpn.* **41** 1 (1989)
38. Pravdo S H, Ghosh P *Astrophys. J.* **554** 383 (2001)
39. La Barbera A et al. *Astron. Astrophys.* **438** 617 (2005)
40. Kreykenbohm I et al. *Astron. Astrophys.* **427** 975 (2004)
41. Doroshenko V et al. *Astron. Astrophys.* **515** A10 (2010)
42. Quaintrell H et al. *Astron. Astrophys.* **401** 313 (2003)
43. van Kerkwijk M H et al. *Astron. Astrophys.* **303** 483 (1995)
44. Rappaport S *IAU Circ.* **2869** 2 (1975)
45. Bochkarev N G, Karitskaya E A, Shakura N I *Sov. Astron. Lett.* **1** 237 (1975) [*Pis'ma Astron. Zh.* **1** 13 (1975)]
46. Nagase F et al. *Publ. Astron. Soc. Jpn.* **38** 547 (1986)
47. Watanabe S et al. *Astrophys. J.* **651** 421 (2006)
48. Staubert R *Chin. J. Astron. Astrophys.* **3** (Suppl.) 270 (2003)
49. Doroshenko V, PhD Thesis (IAAT) (Tübingen: Institut für Astronomie und Astrophysik Tübingen, Univ. Tübingen, 2011)
50. Davidsen A, Malina R, Bowyer S *Astrophys. J.* **211** 866 (1977)
51. Hinkle K H et al. *Astrophys. J.* **641** 479 (2006)
52. Makishima K et al. *Nature* **333** 746 (1988)
53. Dotani T et al. *Publ. Astron. Soc. Jpn.* **41** 427 (1989)
54. Hénault-Brunet V et al. *Mon. Not. R. Astron. Soc.* **420** L13 (2012)
55. Haberl F et al. *Astron. Astrophys.* **537** L1 (2012)
56. Popov S B, Turolla R *Mon. Not. R. Astron. Soc.* **421** L127 (2012)
57. Fu L, Li X-D *Astrophys. J.* **757** 171 (2012)
58. Reig P, Torrejón J M, Blay P *Mon. Not. R. Astron. Soc.* **425** 595 (2012)
59. Ribó M et al. *Astron. Astrophys.* **449** 687 (2006)
60. Torrejón J M et al. *Astron. Astrophys.* **423** 301 (2004)
61. Masetti N et al. *Astron. Astrophys.* **423** 311 (2004)
62. Blay P et al. *Astron. Astrophys.* **438** 963 (2005)
63. Wang W *Mon. Not. R. Astron. Soc.* **398** 1428 (2009)
64. Raymond J C, Cox D P, Smith B W *Astrophys. J.* **204** 290 (1976)
65. Cowie L L, McKee C F, Ostriker J P *Astrophys. J.* **247** 908 (1981)
66. Tarter C B, Tucker W H, Salpeter E E *Astrophys. J.* **156** 943 (1969)
67. Hatchett S, Buff J, McCray R *Astrophys. J.* **206** 847 (1976)
68. Sunyaev R A, Shakura N I *Sov. Astron. Lett.* **3** 138 (1977) [*Pis'ma Astron. Zh.* **3** 262 (1977)]
69. Marykutty J et al. *Mon. Not. R. Astron. Soc.* **407** 285 (2010)
70. Ducci L, Sidoli L, Paizis A *Mon. Not. R. Astron. Soc.* **408** 1540 (2010)
71. Chashkina A, Popov S B *New Astron.* **17** 594 (2012)
72. Landau L D, Lifshitz E M *Fluid Mechanics* (Oxford: Pergamon Press, 1987) [Translated from Russian: *Gidrodinamika* (Moscow: Nauka, 1986)]
73. Wasiutyński J *Studies in Hydrodynamics and Structure of Stars and Planets* (Oslo: Dybwad, 1946)
74. Shakura N I, Sunyaev R A *Adv. Space Res.* **8** 135 (1988)
75. Shakura N I, Sunyaev R A, Zilitinkevich S S *Astron. Astrophys.* **62** 179 (1978)
76. Parker E N *Interplanetary Dynamical Processes* (New York: Interscience Publ., 1963)
77. Beskin V S *MHD Flows in Compact Astrophysical Objects* (Heidelberg: Springer, 2010) [Translated from Russian: *Osesimmetrichnye Statsionarnye Techeniya v Astrofizike* (Moscow: Fizmatlit, 2005)]